Monthly Notices of the ROYAL ASTRONOMICAL SOCIETY

MNRAS **469,** 3688–3712 (2017) doi:10.1093/mnras/stx1085
Advance Access publication 2017 May 6

The Catalina Surveys Southern periodic variable star catalogue

A. J. Drake,[1]★ S. G. Djorgovski,[1] M. Catelan,[2,3] M. J. Graham,[1] A. A. Mahabal,[1] S. Larson,[4] E. Christensen,[4] G. Torrealba,[5] E. Beshore,[4] R. H. McNaught,[6] G. Garradd,[6] V. Belokurov[5] and S. E. Koposov[5]

[1]*California Institute of Technology, 1200 E. California Blvd, CA 91225, USA*
[2]*Instituto de Astrofísica, Pontificia Universidad Católica de Chile, Facultad de Física, Av. Vicuña Mackena 4860, 782-0436 Macul, Santiago, Chile*
[3]*Millennium Institute of Astrophysics, Vicuña Mackenna, 4860, Santiago, Chile*
[4]*Department of Planetary Sciences, Lunar and Planetary Laboratory, The University of Arizona, 1629 E. University Blvd, Tucson, AZ 85721, USA*
[5]*Institute of Astronomy, Madingley Road, Cambridge CB3 0HA, UK*
[6]*The Australian National University, Acton, ACT 2601, Australia*

Accepted 2017 May 2. Received 2017 April 27; in original form 2017 February 27

ABSTRACT

Here, we present the results from our analysis of 6 yr of optical photometry taken by the Siding Spring Survey (SSS). This completes a search for periodic variable stars within the 30 000 deg^2 of the sky covered by the Catalina Surveys. The current analysis covers 81 million sources with declinations between -20° and -75° with median magnitudes in the range $11 < V < 19.5$. We find approximately 34 000 new periodic variable stars in addition to the ∼9000 RR Lyrae that we previously discovered in SSS data. This brings the total number of periodic variables identified in Catalina data to ∼110 000. The new SSS periodic variable stars mainly consist of eclipsing binaries, RR Lyrae, LPVs, RS CVn stars, δ Scutis, and Anomalous Cepheids. By cross-matching these variable stars with those from prior surveys, we find that ∼90 per cent of the sources are new discoveries and recover ∼95 per cent of the known periodic variables in the survey region. For the known sources, we find excellent agreement between our catalogue and prior values of luminosity, period, and amplitude. However, we find many variable stars that had previously been misclassified. Examining the distribution of RR Lyrae, we find a population associated with the Large Magellanic Cloud (LMC) that extends more than 20° from its centre confirming recent evidence for the existence of a very extended stellar halo in the LMC. By combining SSS photometry with Dark Energy Survey data, we identify additional LMC halo RR Lyrae, thus confirming the significance of the population.

Key words: stars: variables: general – stars: variables: RR Lyrae – Galaxy: halo – Galaxy: stellar content – Galaxy: structure.

1 INTRODUCTION

Periodic variable stars provide a wealth of information ranging from stellar interiors to the cosmological distance scale (e.g. Catelan & Smith 2015). The nature of the sources has been studied for hundreds of years. However, the advent of large-scale microlensing surveys, such as massive compact halo object (Alcock et al. 1993) and Optical Gravitational Lensing Experiment (OGLE; Udalski et al. 1994), revolutionized this work by greatly increasing the quantity and quality of variable star information. Nevertheless, the coverage of the microlensing surveys was limited to the Galactic bulge and the Magellanic Clouds and thus left most of the sky to be explored.

Surveys such as All Sky Automated Survey (ASAS; Pojmanski 1997) began to fill this gap by covering most of the sky with very wide-field cameras that survey most of the sky. This led to the discovery of tens of thousands of variable stars (Pojmanski 2000, 2002, 2003; Pojmanski & Maciejewski 2004a, Pojmanski & Maciejewski 2004b; Pojmanski, Pilecki & Szczygiel 2005). Similarly, surveys for planetary transits (e.g. HATNet, Hartman et al. 2011; the Burrell Optical Kepler Survey, Feldmeier et al. 2011) also discovered large numbers of periodic variable stars over much of the sky. However, all of these initial surveys lacked the depth of the earlier microlensing surveys.

During the past decade additional effort has been made to explore the presence of variability over the entire sky to the moderate limits of the microlensing surveys ($V \sim 20$). Such depth and breadth is required to properly characterize the local variable population as well as the structure of the Galaxy itself. For example, the discovery of RR Lyrae standard candles is currently enabling us to trace the formation and extent of our Galaxy via the locations, velocity, and abundances of tidal streams and other features (Drake et al. 2013a).

★E-mail: ajd@astro.caltech.edu

One of the most promising avenues in this work has been harvesting periodic variable stars from archival data obtained in the search for Near-Earth Objects (NEOs). Data from the Lowell Observatory Near-Earth Object Search (Bowell et al. 1995) was searched by Miceli et al. (2008), while data from the Lincoln Near-Earth Asteroid Research (LINEAR; Stokes et al. 2000) was analysed by Sesar et al. (2013) and Palaversa et al. (2013). Likewise, we have begun to explore data from the Catalina Sky Survey (CSS, Larson et al. 2003). In Drake et al. (2013a,b) and Torrealba et al. (2015), we targeted type-ab RR Lyrae variables, and later extended our search to investigate all types of periodic variable sources in CSS data. In Drake et al. (2014a; DR14 hereafter), we explored the Northern data ($\delta > -20^\circ$, hereafter CSS-N).

In this paper, we extend our investigation to the South by searching for periodic variables from Siding Springs Survey (SSS) data. Specifically, we will catalogue periodic variable stars in the region $-20^\circ < \delta < -75^\circ$ that was not covered by our previous analysis.

2 OBSERVATIONS

The CSS[1] began taking observations using three telescopes in 2003. Each telescope was run as a separate sub-survey. These consisted of the Catalina Schmidt Survey and the Mount Lemmon Survey (MLS) in Tucson, Arizona, and the SSS at Siding Spring, Australia. The aim of this ongoing project is to discover NEOs, with a particular emphasis on those that might be Potentially Hazardous Asteroids.

Each of the Catalina telescopes has observed a grid of fields that tile the local sky. Combined, the surveys cover most of the sky between declinations $\delta = -75^\circ$ and $+65^\circ$. However, regions within $\sim 15^\circ$ of the Galactic plane have generally been avoided due to difficulty of discovering moving objects in very crowded fields. Most of the observations have been taken in sets of four images where each field is repeatedly observed after 10 min. All of the images are unfiltered and have aperture photometry carried out using the SExtractor program (Bertin & Arnouts 1996).

In this paper, we concentrate on the photometry from the SSS taken between 2005 and 2013 (when the Uppsala Schmidt 0.5 m telescope was decommissioned). The SSS images cover 4.2deg^2 on the sky, with each location having $\sim$200 observations. The individual light curves are built by matching detections with objects found from a much deeper 'master' catalogue. These catalogues are derived from photometry performed on a frame built by median combining 20 or more individual SSS images. Although the SSS data cover the region $0^\circ > \delta > -75^\circ$, we restrict our analysis to the 10 000 deg^2 covered by SSS in the region $-75^\circ < \delta < -20^\circ$. Sources in the area $\delta > -20^\circ$, generally have better temporal coverage and depth in the CSS-N data that was previously analysed by DR14. In total, this subset includes $\sim$81 million discrete objects having $11 < V < 20$ and at least 20 observations. All of the photometry that we use is publicly available as part of Catalina Surveys Data Release 2 (CSDR2).[2]

3 VARIABLE SOURCE SELECTION

Our first step in finding periodic variable stars within the SSS data was to select all the candidate variable sources. We followed the same method as we applied to CSS-N data in DR14. This involves making initial selection of variable stars based on values of the Stetson variability index ($J_{\rm WS}$, Stetson 1996) along with the weighting scheme of Zhang et al. (2003). As with DR14, we remove sources that mimic variability due to intermittent blending. This occurs when close sources are detected as a single object in poor seeing and multiple sources in good seeing. The effect is most notable in the crowded fields near the Galactic plane.

Apart from source blending, there are systematic variations in the photometric scatter observed in different fields. This can also be attributed to crowding in addition to differences in the distribution of airmasses and sky conditions between fields. As with our CSS-N analysis (DR14), we determine a magnitude-dependent $J_{\rm WS}$ threshold to select variables separately from each of the $\sim$2400 SSS fields. Among the initial 81 million SSS sources in the analysed region, 3.4 million objects were selected as candidate variable sources.

3.1 Selection of periodic variables

We searched all 3.4 million variable the variable star candidates for possible periodic sources using Lomb–Scargle (LS, Lomb 1976; Scargle 1982) periodogram analysis. As with DR14, we selected candidate periodic sources based on an LS periodic significance statistic of $\eta < 10^{-5}$. This selection netted us $\sim$360 thousand candidates (or $\sim$0.4 per cent of the input source catalogue).

We then ran the adaptive Fourier decomposition (AFD) method (Torrealba et al. 2015) on each of the candidate periodic variable stars. The AFD technique improves the selection by comparing Fourier fits to the five best periods found by LS along with five periods from each of regular bin Analysis of Variance (AoV) and multiharmonic AoV (Schwarzenberg-Czerny 1996). In this process, we used multiple period-finding techniques since the accuracy and completeness of each method varies significantly depending on the type of variability and sampling (Graham et al. 2013). The combination of three different period-finding techniques increases the chance of finding the true period and provides confidence when a common period is found with multiple different techniques.

As expected from our prior work, a fraction of the sources analysed had best-fitting AFD periods (P) that were found to be artefacts of the sampling pattern, or sky brightness variations with lunar phase. These effects lead to period estimates that are fractions and multiples of a sidereal day, or values near sidereal and synodic months. We examined the light curves of many sources clustered around these periods and removed candidates within narrow ranges of the spurious periods. The side effect of removing these candidates is that small number genuine periodic variables matching these values can also be inadvertently removed. However, based on the density of sources and the very small period ranges, we expect these to be <1 per cent of all genuine periodic variables. In addition, we removed objects that had both poor Fourier fits to their phased light curves ($\chi^2_r > 5$) and low periodic significance ($\eta < 10^{-9}$). These combined cuts reduce the number of periodic variable candidates to $\sim$270 thousand.

Investigating the distribution of AFD periods for the remaining sources, we found $\sim$130 thousand candidates that had best periods of $P > 1000$ d. Each SSS light curve spans up to 8 yr, so it is possible to find such long periods. However, inspection of a few hundred of these objects showed them to be aliases of half the time span of the data. In most cases, the false periodicity is caused by a small amount of erroneous photometry taken near the beginning of the survey. However, some of the sources matched known QSOs. Such sources are generally seen to exhibit variability, and only very occasionally periodicity (Graham et al. 2015). Based on surveys

[1] http://www.lpl.arizona.edu/css/
[2] http://catalinadata.org

with much longer baselines than ours, we expect very few genuine periodic sources with $P > 1000$ d. For example, Soszyński et al. (2013) found that <0.2 per cent of long-period variables (LPVs) have $P > 1000$ d in OGLE survey Galactic bulge fields. Very few other types of variables are known to have such long periods. Therefore, we decided to only select candidates having periods <1000 d.

Our initial analysis also revealed many sources with $P > 2$ d that had low values of significance. Inspection of these sources suggests that most are either noise or irregular variables. To deal with these objects, we compared the values of χ^2_r from their Fourier fits to the value based on a constant. We removed ∼10 000 candidates where the improvement in χ^2_r between the Fourier fit and a constant value was insignificant.

4 ANALYSIS

In DR14, we demonstrated how different types of periodic variables were well separated in terms of their colour and periods. That analysis benefitted from the large sky coverage and accurate photometry of SDSS along with *Wide-field Infrared Survey Explorer* (*WISE*) data . In the Southern sky ($\delta < -20^\circ$), there is very little SDSS data. Nevertheless, the availability and coverage of the AllWISE catalogue (Mainzer et al. 2011) allows us to use period and colour information to broadly separate distinct types of variability.

We matched the ∼130 thousand variable candidates with the AllWISE catalogue using the Infrared Processing and Analysis Center matching services. Of these, ∼111 thousand sources had matches within 5″. Investigation of the ∼19 thousand SSS sources without matches revealed many sources that were blended in the *WISE* images. This was expected since the resolution of *WISE* is only 6″–12″ (depending on band), while the resolution of SSS is closer to 4″ (depending on seeing). However, many unmatched sources were simply too faint in the near-infra-red (NIR) to be detected by *WISE*. A small fraction were also missing due to saturation of bright sources in the *WISE* NIR images.

4.1 Automated pre-classification

Future wide-field sky surveys such as the Large Synopic Survey Telescope (LSST) are expected to reveal millions of variable sources in the next decade (Ivezic et al. 2008). Such large numbers significantly hinder the prospects for human classification of variability. With this in mind, over the past decade a number of variability surveys have investigated applying automated classification to such sources. For example, Dubath et al. (2011) applied Random Forest classification to *Hipparcos* data, while Richards et al. (2012) applied the same general technique to techniques to automatically classify variable stars from the ASAS survey. In contrast, Palaversa et al. (2013) used support vector machine (Cortes & Vapnik 1995) based machine learning to classify periodic variables from the LINEAR survey, and Elorrieta et al. (2016) have found that the AdaBoost technique (Freund & Schapire 1997) provides encouraging results in the case of the NIR light curves obtained by the Vista Variables in the Vía Láctea survey (Minniti et al. 2010).

The process of source classification, whether human-based or automated, requires a significant amount of prior knowledge. In DR14, we discovered 47 thousand periodic variables in CSS-N data. Since the CSS-N data are observed and calibrated with the same methods as SSS data, these sources serve as a useful training set for a more automated analysis.

4.1.1 *Parameter and class selection*

In order to determine the prospects for an automated classification approach, we investigated the relative strength of various parameters in separating the main types of variability that were observed in the DR14 data set. We restricted our selection process to use pairs of parameters since the natural sparseness of data when projected into higher dimensions (i.e. the curse of dimensionality) does not allow us to define well-populated groups. Since periodic variable star types are well known to separate into groups with a well-defined period ranges, it was clear that the most powerful discriminator for a given variability type is the period. Therefore, we used this as the primary parameter in our tests.

In order to produce well-defined groups of variables, we restricted our initial classification to objects with periods less than a day. This is because in DR14, we found more than 95 per cent of periodic variables in CSS-N fields had periods less than one day. Objects with longer periods were simply classified by eye.

Based on DR14, the variable stars with periods less than a day are predominately contact binaries, RR Lyrae, and detached eclipsing binaries. Thus, we expected that these would also be the main classes within the SSS data. However, as SSS observations are typically a magnitude shallower than CSS-N observations, different fractions are expected. Furthermore, since SSS took data closer to the Galactic plane and bulge than CSS-N, additional variations are expected.

One important point to consider in the classification process is having well-sampled classes of objects. Although we have a very large number of variable candidates in SSS and CSS-N data, the largest class of variable objects are those without any clear period. This situation contrasts with many automated classification experiments, where in many cases the classification has been undertaken using a pre-selected catalogue of periodic variables (e.g. Dubath et al. 2011; Richards et al. 2012). In such cases, one can assume that almost all of the input sources will indeed be periodic variables. However, this is generally not the case for surveys that aim to find and classify sources that reach the detection threshold (where neither variability nor periodicity are guaranteed). Indeed, Masci et al. (2014) noted the importance of visual inspection in cases where the automated classification is ambiguous due to low signal-to-noise ratio (S/N).

In this analysis, as with DR14, we select these objects using a low threshold for variability and periodicity in order to maximize detection completeness. It is natural to expect that most of the sources initially selected will also not be periodic variables. Therefore, in addition to the genuine variable classes, we add a class for sources that are not truly periodic.

Based on our investigation of correlations between parameters for periodic variables from the CSS-N catalog, we selected the following features for classification: period (P), colour ($V - W1$), M-test statistic (M_t, Kinemuchi et al. 2006, equation 8), amplitude of first component of the Fourier decomposition (A_1), LS periodic significance (η), the goodness-of-fit statistic (χ^2_r), and average variation (Av_σ). This set is similar to the best set of parameters found by Dubath et al. (2011). However, there are some clear differences. For example, Dubath et al. found absolute magnitude to be a useful parameter. However, absolute magnitude is not known for most stars, and thus is generally not available for classification.

We note that our value of M_t is as used by Drake et al. (2013a) and is based on the fit to the light curve rather than sum of the values for the data points. The M_t parameter itself is a measure of the fraction of time that a variable is below the mean magnitude compared to above it. For example, a sinusoidal variable star (such as contact binaries) spend equal time above and below the mean and has an M_t

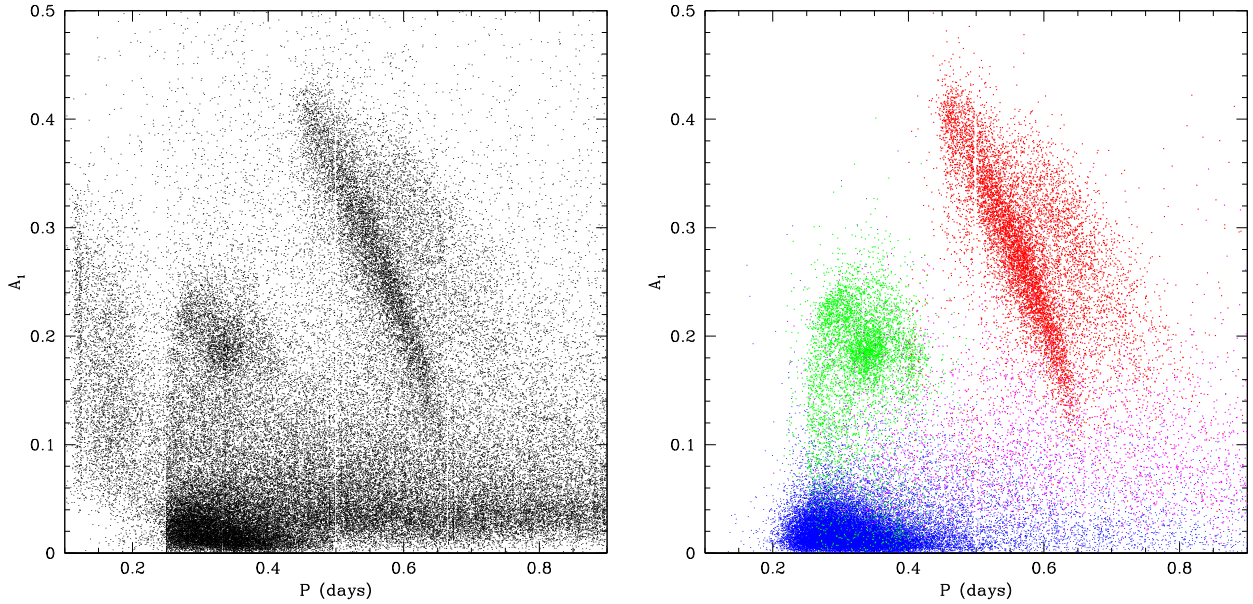

Figure 1. Period–amplitude diagrams of periodic variables. The left-hand panel shows the periodic variable candidates from SSS data before MKDE classification. The right-hand panel shows colour-coded periodic variables from DR14. The blue points show contact binaries, green c-type RR Lyrae, red ab-type RR Lyrae, and magenta detached eclipsing binaries. In the left-hand plot, the points with periods <0.24 d are contact binaries found at their half-periods (see the text for details).

value close to 0.5. In contrast, RRab's generally have $M_t > 0.5$ (and longer periods), while RRc's have M_t values near 0.4. The effect of M_t is similar to that of non-parametric skew, which is effective in separating eclipsing binaries from other types of variables (see for example Richards et al. 2011; Dubath et al. 2011). However, M_t is also useful for separating other types of variables from each other.

The values of the P, η, M_t, A_1, and χ^2_F parameters are all provided by Automatic Period Selection (APS) (Torrealba et al. 2015). On the other hand, Av_σ is the average absolute deviation of the light curve from the median based on the photometric uncertainty, that is:

$$Av_{n\sigma} = \Sigma_i^n |(V_i - V_{\rm med})/\sigma_i|/n, \quad (1)$$

where σ_i is the photometric uncertainty for measurement V_i and median magnitude $V_{\rm med}$, and n is the number of measurements. This parameter essentially represents an average S/N of the variability. The more variable the object, the more each individual measurement will tend to vary from the median. However, due to the presence of occasional errors in the photometry (caused by such things as image artefacts), we exclude measurements greater than 10σ from the median in the calculation.

4.1.2 Multivariate kernel density estimation

After considering a number of automated classification techniques, we decided to use multivariate kernel density estimation (MKDE, Scott 2015). This allows us to simply classify sources based on their parameter space location relative to the CSS-N sample, which we know should have similar properties due to the similarity of the observing and analysis.

In this process, the similarity of points is determined by finding the distance between a test source and each classified object. In this analysis, we define the distance metric in terms of the estimated uncertainty in each of the parameters. However, since the uncertainty is not well defined for all parameters, in cases where the uncertainty is unknown we estimate it based on the distribution of values.

As P is by far the most distinctive parameter for many types of periodic variables, in most cases we found it best to use bivariate classifications by pairing P with another feature. The five pairs of parameters we selected are P versus each of $V - w1$, M_t, A_1, and η, along with χ^2_r versus $Av_{n\sigma}$. For each pair of parameters, we determine the likelihood of each of the five classifications based on our CSS-N priors. These classes are RRab, RRc, Algol-type eclipsing binaries (EA), other non-EA eclipsing binaries (Ecl), and noise (aperiodic or non-variable sources). To classify each candidate, we considered all the previously classified CSS-N objects that lie within 3σ of the candidate.

In Fig. 1, we plot the periods and first component of Fourier series fit for the periodic variable candidates and the sources from DR14. We see that, since contact binaries have two peaks per period, they have small A_1 values, while RRc's have larger values. The SSS data reveal many candidates with $P < 0.24$ d having moderately large amplitudes. These are generally contact binaries where the best-fitting period was half the actual period. These sources were classified by eye and not included in the pre-classification process.

In Fig. 2, we plot the periods versus the LS periodic significance. Clearly there is significant overlap between RRc and contact binaries that does not affect the longer period RRab's. The RR Lyrae tend to have higher average LS significance than the binaries, since the amplitudes of binary star light curves depend on their inclination relative to the line of sight.

In Fig. 3, we plot the periods versus the M_t statistics for each candidate. This shows that the main types of variables are relatively well separated. That is, RRab's generally have $M_t > 0.5$, contact binaries have $M_t < 0.45$, and RRc's $M_t \sim 0.5$. In this plot, we see that the detached binaries have much smaller M_t values than the other sources since their eclipses are always negative deviations from their median brightness. This is probably the strongest discriminator for these sources since the evident halo of noise sources among the raw candidates tend to be characterized by larger values of M_t.

In Fig. 4, we plot the period versus $V_{\rm CSS} - W1$ colour for the periodic candidates. As expected, the contact binaries are generally

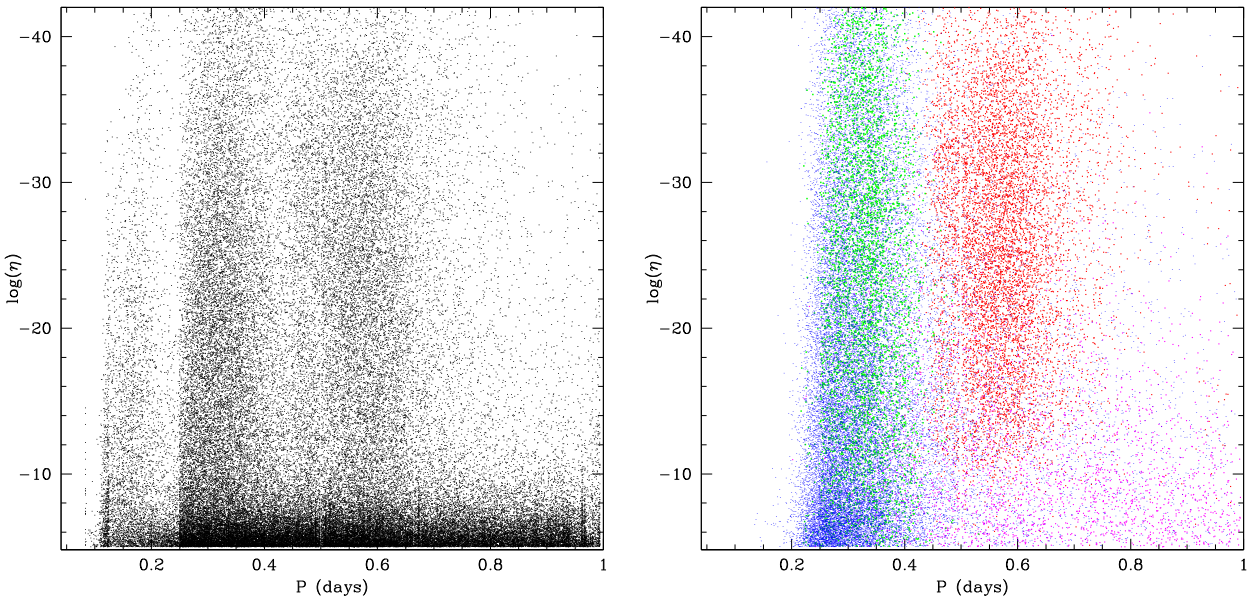

Figure 2. Period–significance plots. On the left, we present the values unclassified SSS periodic variable candidates. On the right, we plot the values for periodic variables in DR14. The source colours are the same as given in Fig. 1.

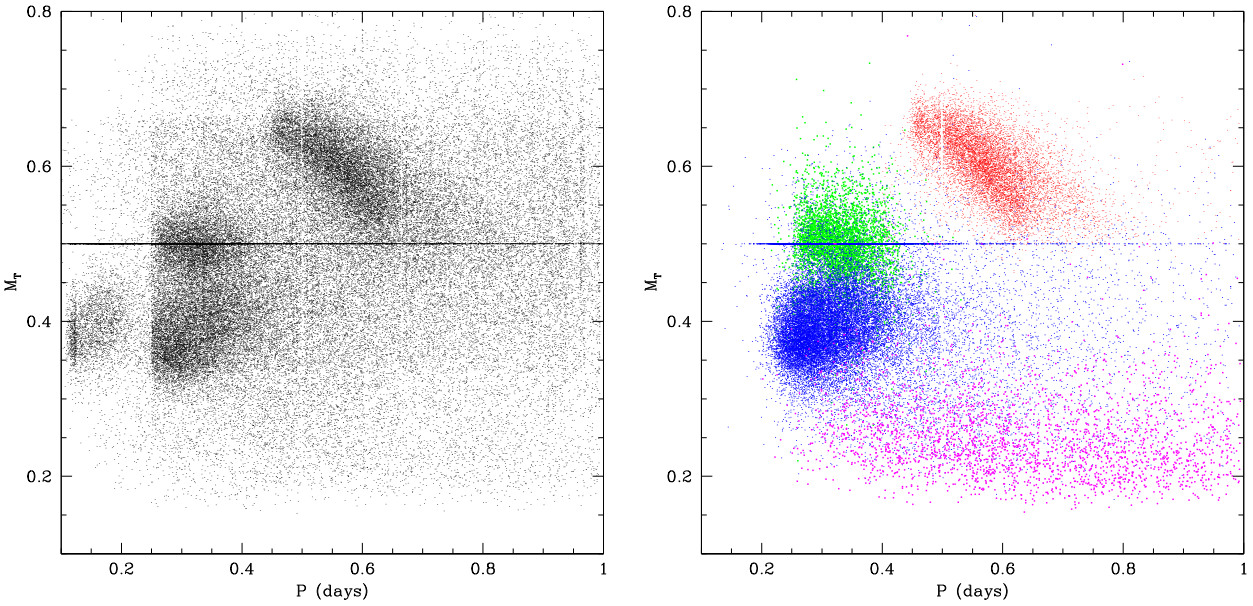

Figure 3. The period–*M*-test statistic distribution. The left-hand panel shows the values for the initial periodic variables candidates from SSS before classification. The right-hand panel shows values for periodic variables in DR14. The colours are as given in Fig. 1.

redder than the RR Lyrae and the groups are quite well separated. We have not plotted the values for detached binaries from DR14 since they exhibit a broad range of periods and colours. The sequence of contact binaries that fold at half their true periods is very evident at $P < 0.24$ d.

In Fig. 5, we plot the goodness of fit (χ^2_r) for the Fourier series fits versus $Av_{n\sigma}$ based on DR14 data. As expected, this plot shows that most of the truly periodic variables are well fitted with a Fourier series (even when they have large amplitudes), while aperiodic sources have poorer fits. We note that many of the sources have $\chi^2_r <$ 1 since the photometric uncertainties are generally overestimated in SSS data.

To determine the best classification of each object, we average the probabilities based on each pair of parameters. For each candidate, we choose the type with the highest probability as the best classification. However, this is not ideal since it is likely that some pairs of parameters have greater significance than others. A better solution might have been to weight the probabilities based on the variances.

To improve the robustness of the process, we thus decided to only use classifications that were based on 10 or more objects of known class. Sources with fewer matches were marked as objects of unknown type. Additionally, since the value of the LS periodic significance, is dependent on the number of measurements, we did not use values from the P versus η parameter distribution for classifying objects that had less than 125 measurements. We also excluded classifications where any of the individual tests suggested a probability <1 per cent. For example, if one pair of parameters shows

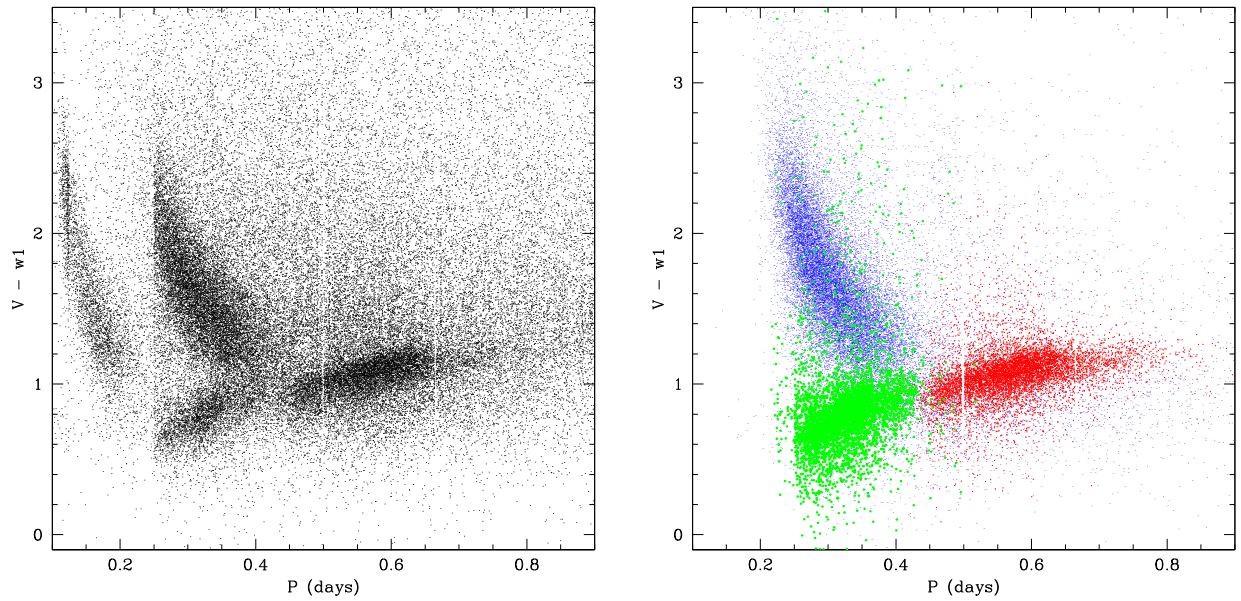

Figure 4. Period–colour distributions. The left-hand panel presents the values of best-fitting periods from AFD and $V_{CSS} - W1$ colour for new periodic variable candidates before classification. The candidates with $P < \sim 0.25$ d are generally those found at half their true periods. The colours are as given as in Fig. 1. In the right-hand panel, those from DR14. The detached binaries have been omitted for clarity.

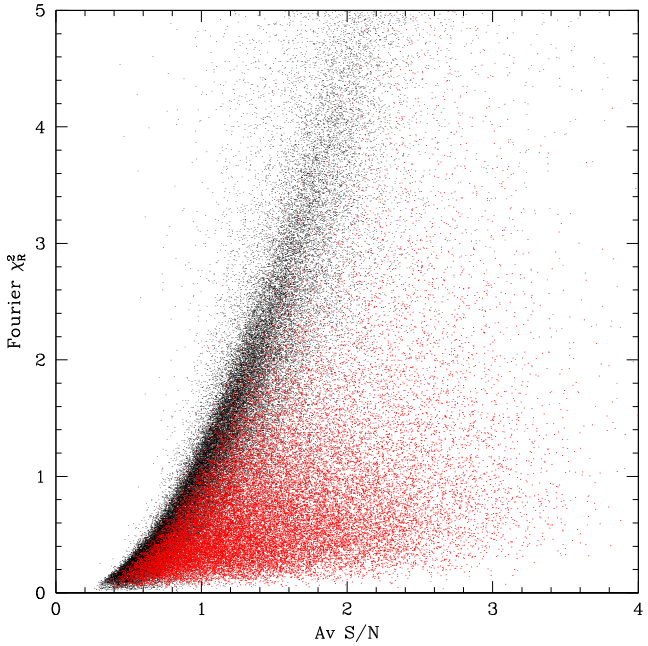

Figure 5. The average variability significance A_V, versus the AFD goodness of fit χ^2_r for variability candidates from DR14. The black points show the sources that were not found to be periodic, while the red points show those that were.

that a particular classification is >80 per cent likely, but another test gave <1 per cent, we left the source as class unknown. The result of these requirements was that only ∼84 000 of the candidates were given an initial classification estimate.

5 FINAL CLASSIFICATION AND VERIFICATION

As noted earlier, in Torrealba et al. (2015) we already selected and classified 10 540 sources as RRab's based on the SSS data. We removed these sources from our list of candidates requiring classification.

The next step was to verify the classifications based on the MKDE estimates. In order to do this, all of the phased light curves for the 119 000 periodic candidates were visually inspected (by AJD). During the process candidates were separated based on their MKDE classification type and ranked by probability. This ordering aids the human classification process since the incorrectly classified sources are those given lowest probability of being within a given class. As expected, most of the objects that were reclassified to other classes generally had similar probabilities of being from more than one class.

All of the objects without an initial MKDE classification were inspected separately of those given a class. Among these, most of the genuine periodic variables were the longer period objects not included in the pre-classification step. All of the candidates that were assessed to have questionable periodicity were placed in the noise class.

Due to the subjective nature of visual inspection, it is likely that some observational biases exist. For example, it is likely that there are candidates where the best-fitting periods from AFD are aliases of the true period. This could lead to the genuine periodic variable either appearing to be aperiodic or from another class of periodic variables. This is particularly likely to be the case when long-period contact binaries are assigned to the RRc class due to the best period being half the true value. However, we inspected the harmonic frequencies for many of the candidates in order to minimize this effect. The inclusion of colour information in the automated pre-selection process should reduce the number of thus misclassified variables.

In total, ∼37 000 of the candidates were classified as periodic variables. These sources have an average of 223 photometric measurements each. In Table 1, we show the effect of each selection on the final number of periodic variables. Only 31 sources we found to be duplicates due to overlap between SSS fields. The catalogue also includes 64 sources that were previously been classified as RRab's in Torrealba et al. (2015). Most of these have the same

Table 1. Periodic variable selection. Selection and objects. Column (1), selection used to reduce the sample of candidate variables. Column (2), number of objects following the sub-selection. These numbers do not include the RRab's previously discovered by Torrealba et al. (2015).

Selection	Objects
SSS sources $\delta < -20^\circ$	$\sim 81 \times 10^6$
Variable candidates	$\sim 3.4 \times 10^6$
LS $\eta < 10^{-5}$	$\sim 365\,000$
$N_{\rm blend} < 5$ per cent plus $P \neq P_{\rm alias}$	$\sim 270\,000$
$P < 1000$ d	$\sim 140\,000$
$\chi^2_{\rm Fourier} < \chi^2_{\rm line}$	$\sim 130\,000$
Previously known SSS RRab's	$\sim 10\,000$
Inspected	$\sim 119\,000$
Periodic	37 745

period in Torrealba et al. (2015), but since they present evidence of additional periodicities (as expected with RRd's) or light-curve modulations (suggestive of the presence of Blazhko effect), their original classifications have been modified here.

In Table 2, we give a comparison between the initial class found using MKDE and the final classification. In Fig. 6, we plot the fraction of correctly classified sources (based on inspection) for each type as a function of average apparent magnitude. This figure shows that the number of correctly classified sources is generally lower for the brightest and faintest sources. This is because the bright sources are affected by saturation, while the faint ones have lower S/Ns.

Overall, we see that more than half of the sources that were initially assigned an EA classification were determined not to be periodic variables at all. This is most likely due to the fact that both EAs and the aperiodic sources exhibit a wide range of colours and potential periods. Only two-thirds of the classifications in the contact binary class were found to be correct. This result is similar to Palaversa et al. (2013) who found 57 per cent with their supervised classification algorithm.

The fraction of correctly classified RRab's is lower than in Palaversa et al. (2013), who found 84 per cent. Counterintuitively, Fig. 6 shows that the number of variable star candidates that were correctly classified as RRab's actually increases with decreasing brightness. The reason for this is that this work does not include any of the bright RRab's found by Torrealba et al. (2015). Most of the bright RRab's have thus already been found and removed from this analysis. If the Torrealba et al. (2015) were included, we expect ∼90 per cent would have been correctly classified. The fraction

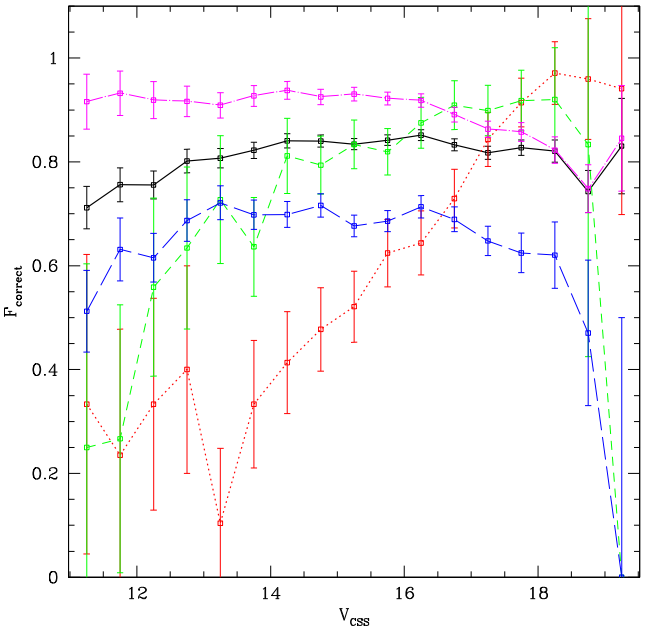

Figure 6. The fraction of correctly classified sources compared with source brightness. The plot lines represent the following classes: solid black lines, all sources; dotted red, RRab's; short-dashed green, RRc's; long-dashed blue, EW's; and dot–dashed magenta, noise sources. The detached (EA) binaries are not plotted due to the large uncertainties associated with the small number of sources. The plotted errors assume Poisson-distributed uncertainties.

of RRc's given the correct classification is similar to that found in Palaversa et al. (2013). The most accurately classified class we found is the aperiodic noise sources. Among these, 91 per cent were placed in the correct class. This is probably due to the low values of periodic significance that define most of these objects.

Overall, we see that had we adopted the initial MKDE classifications as the ground truth, hundreds of RRab's and thousands of eclipsing binaries would have been missed from the catalogue and thousands would have been misclassified. This result strongly suggests that more work is required to automatically select and classify periodic variables when low detection thresholds are applied.

6 TYPES OF VARIABLES

Following DR14, the SSS periodic variables can generally be classified into three broad classes: eclipsing, pulsating, and rotational.

Table 2. Comparison between pre- and final classifications. This table contains the confusion matrix for the classifications in this paper, with the first five lines showing number fractions and the last five the corresponding absolute values. It compares objects assigned to the five initial MKDE classes with the final catalogue class both in terms of their fraction and absolute numbers. The periodic variable types are as noted in the text.

Type	RRab	RRc	RRd	Blaz	Ecl	EA	ROT	LPV	DS	ACEP	Misclassified	Cep	Noise	Total
RRab	0.72	0.06	0.02	0.03	0.05	0.03	0.02	0.00	0.00	0.01	0.01	0.00	0.06	1.00
RRc	0.00	0.84	0.05	0.00	0.07	0.00	0.03	0.00	0.00	0.00	0.00	0.00	0.01	1.00
Ecl	0.02	0.02	0.01	0.00	0.68	0.06	0.09	0.00	0.00	0.01	0.01	0.00	0.10	1.00
EA	0.03	0.00	0.00	0.00	0.03	0.37	0.01	0.00	0.00	0.00	0.01	0.00	0.53	1.00
Noise	0.01	0.00	0.00	0.00	0.03	0.03	0.01	0.00	0.00	0.00	0.00	0.00	0.91	1.00
RRab	1913	157	45	67	134	70	60	0	0	24	25	6	173	2674
RRc	6	2897	169	0	225	0	87	0	0	0	14	2	40	3440
Ecl	294	275	225	44	12490	1125	1701	9	29	100	134	23	1832	18281
EA	55	0	1	7	60	652	26	4	0	3	21	0	937	1766
Noise	495	99	34	42	1526	1476	707	3	13	8	66	4	43398	47871

Table 3. Periodic variable star frequency. This table gives the number of periodic variables in each class in the catalogue. A numerical 'Label' is used to associate the entries in the machine-readable catalogue with their classifications. This table includes 28 sources that were detected in multiple times due to a small overlap between fields.

Type	*N*	Label
Ecl	18 803	5
EA	4509	6
RRab	4325	1[a]
RRc	3752	2
RRd	502	3
Blazhko	171	4
ROT	3636	7
LPV	1286	8
DS	147	9
ACEP	153	10
Cep-II	153	12
LMC-Cep	10	13
Miscellaneous	298	11

Note. [a]Excludes ∼10 500 known SSS RRab's from Torrealba et al. (2015).

The pulsating sub-types that we consider can include δ Scutis, RR Lyrae, Cepheids, Mira, and semiregular variables.

The RR Lyrae class consists of RRab's (fundamental mode), RRc's (first overtone mode), and RRd's (multimode). However, many RR Lyrae are known to exhibit the Blazhko effect (long-term modulation; Blazhko 1907). We have chosen to divide objects exhibiting this effect into a separate 'class'. In SSS data, the Cepheids include type-II (Cep-II), Anomalous Cepheids (ACEPs), and Classical Cepheids. We include both semiregular variables and Mira variables under a single, LPV classification. For a more detailed description of the properties of these and other types of pulsating stars, the reader is referred to the recent monograph by Catelan & Smith (2015).

The eclipsing variables in the SSS data were generally divided into a contact plus semidetached binary group (Ecl), and detached systems (EA), class. The separation of eclipsing binary types is often not clear. This is particularly the case when their light curves have a low S/N. Therefore, unlike DR14, we did not attempt to divide the contact (EW) and semidetached binaries (EB) parametric fits to all of the eclipsing binaries light curves, such as performed by Lee (2015) and Marsh et al. (2016) on DR14 binaries, should provide a more objective and quantitative separation for all eclipsing binary classes.

The variable stars that we observed from the rotating variable class include ellipsoidal variables (ELL) and spotted (RS CVn, BY Draconis, and FK Comae) systems. We do not distinguish between these types of variable stars since they typically have low amplitudes (<0.2 mag), making the division unclear. For example, stars with a relatively concentrated and stable system of spots and those with ellipsoidally distorted envelopes can both appear to vary in an approximately sinusoidal manner. Here, we simply include these types in a combined rotational (ROT) class.

As with DR14, a small group of periodic variables exhibiting distorted light curves and varying minima and maxima were discovered. Since the nature of these variable stars is unclear, we place them in the miscellaneous variables class. We also place compact binaries, such as white dwarfs (WDs) and sub-dwarfs in binaries with main-sequence (MS) companions, in this group. The small number of sources that are clearly periodic, yet difficult to classify accurately, are similarly labelled.

In Table 3, we present the total number of periodic sources from each class. However, we have not included the RRab's discovered by Torrealba et al. (2015). Table 4 contains the coordinates, periods, brightnesses, amplitudes, and proposed classification for all the periodic variable sources detected in our analysis.

In the following sections, we will briefly discuss the main classes and sub-classes of periodic variables that we found. Since much of this work builds on DR14, we direct the reader to that work for additional examples and details of each variable type.

6.1 Eclipsing binaries

Systems of orbiting stars are seen to eclipse when the plane of their orbit intersects our line of sight. The measurement of some eclipsing binary systems enables the determination of stellar parameters to high degree of accuracy using the geometrical constraints on

Table 4. Periodic variable catalogue. Column (1), SSS ID; Columns (2) and (3), right ascension and declination (J2000); Column (4), period in days; Column (5), average magnitude from AFD; Column (6), number of measurements in SSS light curve; Column (7), fit amplitude from AFD; Column (8), numerical class number based on Table 3; and Column (9), previously known ID from VSX.

SSS ID	RA	Dec. (J2000)	*P* (d)	$\bar{V}_{SSS}$	Npts	A_{VCSS}	Class	Other ID
SSS_J000025.8−393651	00:00:25.81	−39:36:51.0	0.51438	14.70	230	0.26	5	–
SSS_J000031.7−412854	00:00:31.74	−41:28:54.9	0.589281	19.16	145	0.83	1	–
SSS_J000037.9−251101	00:00:37.91	−25:11:01.6	0.616695	17.55	147	0.49	1	–
SSS_J000044.8−430758	00:00:44.81	−43:07:58.8	0.333486	15.20	212	0.37	2	–
SSS_J000049.3−284901	00:00:49.31	−28:49:01.2	0.583042	14.81	196	0.83	1	TZ Scl
SSS_J000111.5−223745	00:01:11.52	−22:37:45.5	1.791890	14.20	120	0.57	6	–
SSS_J000122.5−263525	00:01:22.59	−26:35:25.2	0.773537	13.83	163	1.02	6	UU Scl
SSS_J000139.0−462830	00:01:39.09	−46:28:30.7	0.642698	13.81	206	0.33	5	–
SSS_J000139.1−362128	00:01:39.14	−36:21:28.1	0.266852	14.51	234	0.45	5	1SWASP J000139.04−362125.6
SSS_J000144.6−233633	00:01:44.68	−23:36:33.8	0.372196	15.88	119	0.51	2	–
SSS_J000145.5−353319	00:01:45.53	−35:33:19.9	0.270948	15.30	231	0.56	5	–
SSS_J000215.0−250134	00:02:15.06	−25:01:34.2	0.57106	17.35	129	0.71	1	–
SSS_J000229.5−333623	00:02:29.54	−33:36:23.3	0.284958	16.09	227	0.25	5	–
SSS_J000241.2−304027	00:02:41.21	−30:40:27.8	0.341439	15.87	220	0.55	5	–
SSS_J000247.9−245643	00:02:47.96	−24:56:43.3	0.493355	10.26	129	1.09	1	RU Scl

Note: The full table will be available online.

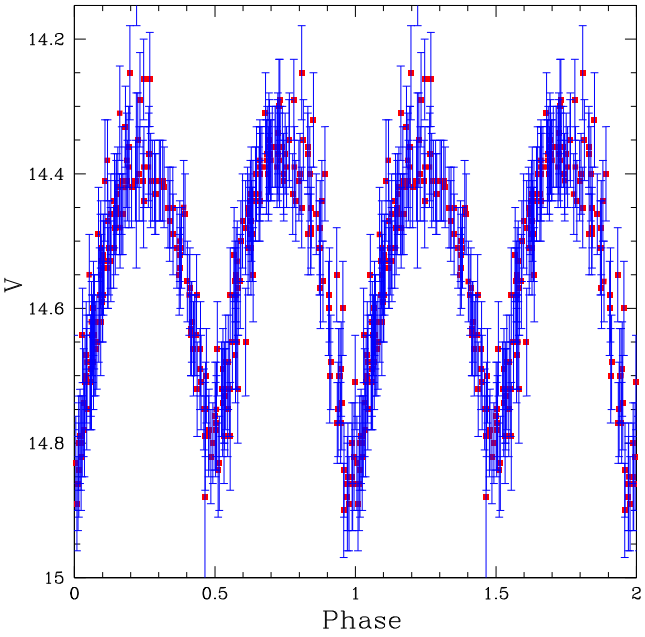

Figure 7. The SSS light curve of contact binary V2215 Sgr. This object has a period of ∼0.26 d and had previously been identified as an RRab based on Gavrilchenko et al. (2014).

the system. For example, under favourable conditions, it is possible to measure the period, inclination, and radial velocity of the stars and thereby determine the radius of each star in the system. Well-constrained systems can also be used to accurately measure distances (e.g. Pietrzynski et al. 2013).

6.1.1 *Contact binaries*

Contact binaries occur when both stars fill their Roche lobes. Eclipsing contact binaries are referred to as both W Ursae Majoris (W UMa's) stars or EW's, after the prototype. The stars in these systems usually have very similar temperatures and spectral types and give rise to eclipses with symmetric shapes. However, slight differences in temperature and size are sometimes present, and give rise to slight differences in eclipse depth. In general, contact binaries have been found to have minimum periods near 0.22 d (Rucinski 1992, 1997). However, a small number of systems with shorter periods have recently been found (e.g. Drake et al. 2014b , and references therein).

In Fig. 7, we present an example of an SSS contact binary light curve, namely V2215 Sgr's. Interestingly, this object is incorrectly classified in the SIMBAD astronomical data base[3] as an RRab star (based on Gavrilchenko et al. 2014). However, the object is correctly classified in the International Variable Star Index (VSX, Watson 2006) based on SuperWasp data (Butters et al. 2010). Since part of this work involves determining the accuracy of our classification, other examples of previously misclassified variables will also be highlighted in the remainder of this paper.

6.1.2 *O'Connell effect binaries*

One of the most poorly understood features of contact binary light curves are cases where the two maxima of the system have different luminosities. Such cases are rare and highly unusual since the stars are viewed side-by-side at the time of maximum. Such asymmetry is called the O'Connell effect (O'Connell 1951). Wilsey & Beaky (2009) reviewed this effect and noted that there are three possible causes: star-spots, gas stream impacts, and circumstellar matter. In the star-spot model, chromospheric and magnetic activity lead to the production of spots on the surface of at least one of the stars. In this scenario, one expects some evolution in the size of the star-spots (as seen in RS CVn binary systems), provided that an activity cycle exists.

At present, few objects are known to exhibit a significant O'Connell effect, and so determining the nature of the variation can clearly be important in revealing its origin. In Fig. 8, we plot the light curves of O'Connell effect binaries with variation in peak brightness of 0.15–0.5 mag. Among these sources we find KK Hya, which Shishayeva & Kholopov (1977) noted as an RR Lyrae. This stars exhibits a 0.5 mag difference in peak brightness between eclipses. As with V2215 Sgr above, this source is clear not an RR Lyrae. In most cases (apart from SSS J042242.7−453029), we see that the peak brightness is followed by the shallowest of the two eclipses.

Our data show that there is a significant diversity among these binaries. The variation between maxima is up to ∼0.7 mag and eclipses up to a magnitude (compared to a maximum of ∼ 0.8 for normal contact binaries). This suggests that, if spots were the cause of the O'Connell effect, an area the size of one of the stars would have to be entirely obscured. Furthermore, as with DR14, we do not see significant variation with time, thus once again suggesting that these sources are stable on time-scales of years. Considering these points, the star-spot explanation does not seem plausible, at least not for all sources. We also note that the scatter in the phased light curves is consistent with that seen in other types of variables of similar brightness. Therefore, it also seems unlikely that obscuration due to a circumstellar gas streams. In such cases, one expects significantly changes in the morphology of the gas cloud over years (corresponding to thousands of orbits). The changes in extinction that these changes cause should introduce scatter into the phase light curves.

6.1.3 *Detached and semidetached eclipsing binaries*

Detached eclipsing binaries correspond to gravitationally bound but well-separated stars whose orbital plane is aligned closely along our line of sight. Unlike contact binaries, these stars can have very different temperatures, resulting in systems with high degree of variability, and eclipses with depths up to ∼3 mag. In Fig. 9, we present an example of a eclipsing EA system, SSSJ070448.8−470426. EAs can also have highly elliptical orbits. In such cases, the primary and secondary eclipse times are generally not equally separated.

In Fig. 10, we present the SSS light curve of VY Dor. Here, we can see that the time of the eclipse ingress and egress are not well defined, and the depths of the primary and secondary eclipses are noticeably different. Such light curves are typical of semidetached (β Lyrae) type eclipsing binaries. However, such systems can be difficult to distinguish from detached systems while those with smaller, more similar eclipse amplitudes are difficult to distinguish from contact systems. This particular source is misidentified as an RR Lyrae variable in SIMBAD, based on the analysis of Tycho data by Mennessier & Colome (2002). Additional examples of EA and EB light curves from Catalina data can be seen in DR14.

[3] http://simbad.u-strasbg.fr/simbad/

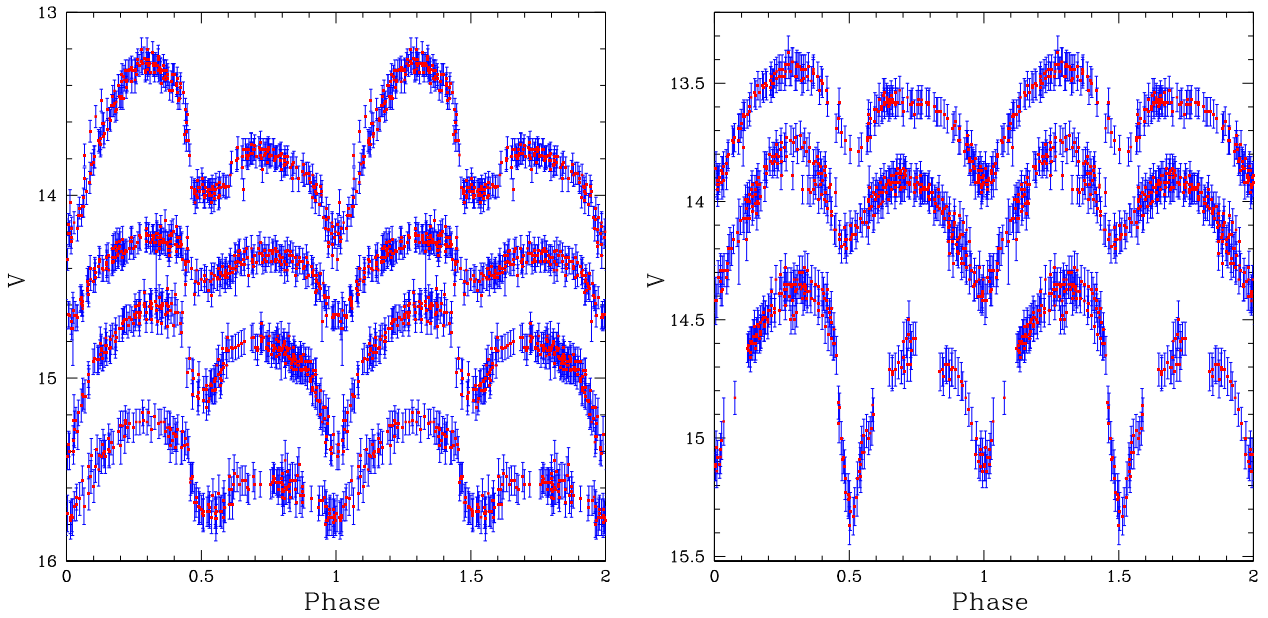

Figure 8. The SSS light curves of O'Connell effect binaries. In the left-hand panel, from top to bottom, we plot the light curves of KK Hya, SSS_J112706.0−290141, SSS_J194510.3−564340, and SSSJ042556.2−473108. In the right-hand panel, from top to bottom, we plot SSS_J074708.9−534552, SSS_J200508.1−502101, and SSS_J042242.7−453029. The objects have periods from ∼0.35 to ∼0.78 d.

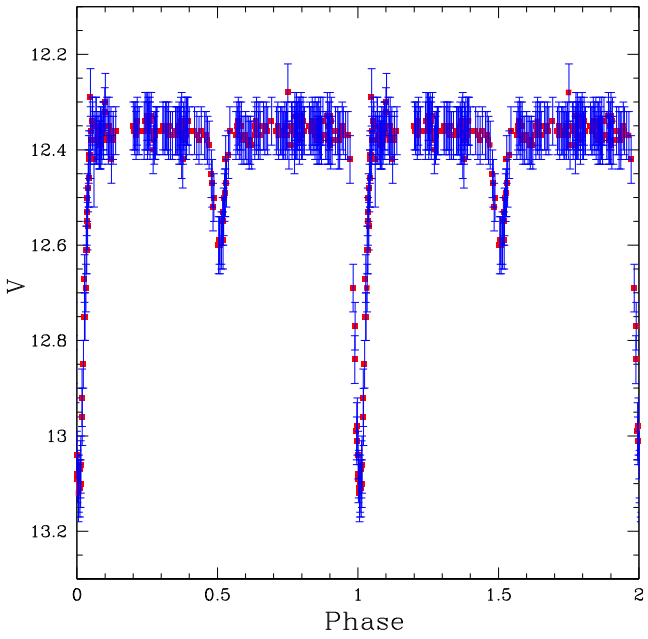

Figure 9. The SSS light curve of detached eclipsing binary candidate SSSJ070448.8−470426. The system has a period of ∼1.66 d.

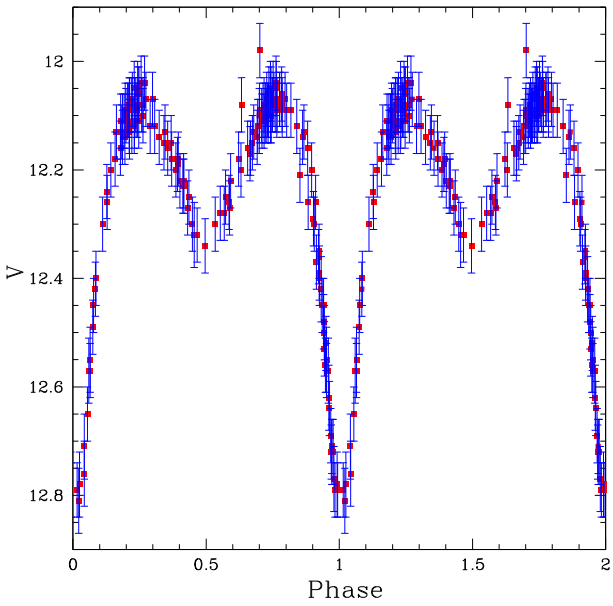

Figure 10. The SSS light curve of VY Dor. A likely semidetached eclipsing binary system with a period of ∼0.497 d.

6.2 Compact eclipsing binary systems

Compact eclipsing binaries include systems with WDs and sub-dwarfs (mainly sdB's and sdO's). Such binaries often exhibit orbital periods less than 0.2 d. This helps distinguish them from contact binaries with similar shapes (Drake et al. 2014b). These post-common-envelope binaries include WD-dM systems, and are related to interacting close binaries such as cataclysmic variables (CVs). Sub-dwarf binaries (HW Vir systems) may also form through a common envelope phase. However, since the MS companions are often highly distorted, this can cause large enough variations that they can be found even if the system is not eclipsing. Similar light curves are also exhibited for γ-ray pulsar binaries such as PSR J2339−0533 (Romani & Shaw 2011) and AY Sex (Wang et al. 2009; Tam et al. 2010).

In Fig. 11, we plot the light curve of SSSJ120928.4−435810. The light curve resembles that of sdB+M binary archetype HW Virginis. The short period (0.174 d) is less than the contact binary minimum. The short eclipse time shows that one of the stars is compact. Further evidence for this classification comes from the significant UV flux (*GALEX* gives FUV = 15.8 and NUV = 16.0; Martin et al. 2005). Thus, the UV colour is consistent with WD+dM binaries (Drake et al. 2014b), and sub-dwarfs (Vennes, Kawka & Nemeth 2011).

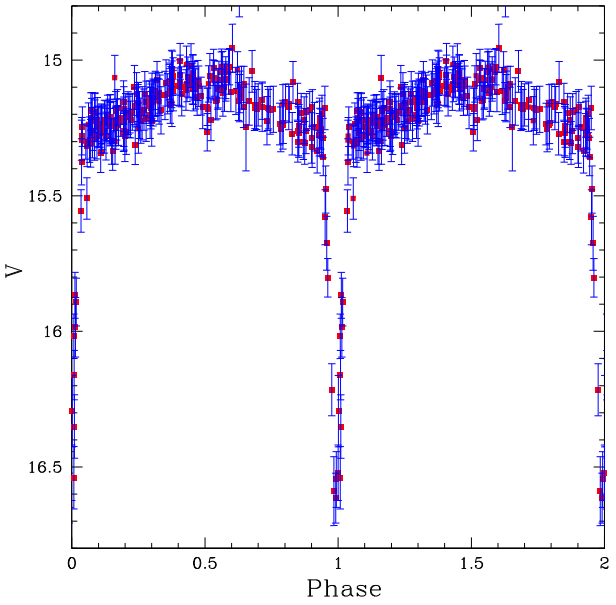

Figure 11. The SSS light curve of compact binary candidate SSSJ120928.4−435810 phased with a period of ∼0.174 d.

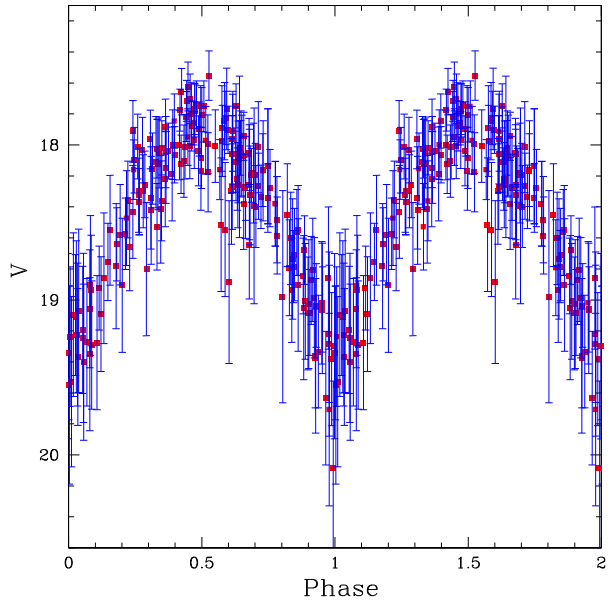

Figure 12. The SSS light curve of redback pulsar candidate 1FGL J0955.2−3949, The source has a period of 9.3 h.

In Fig. 12, we plot the light curve of SSSJ095527.8−394752. This object matches *Swift* telescope X-ray source SWXRT J095527.8−394750. The source is linked to *Fermi* γ-ray source 1FGL J0955.2−3949 by Paggi et al. (2013). We initially identified this source as a possible Redback type (see Roberts 2013) millisecond pulsar binary in 2012 as part of our search for periodic sources associated with unidentified *Fermi* γ-ray sources (e.g. Bellm et al. 2016). Based on the very large amplitude ($\Delta V \sim 1.5$ mag), the shape, and the period (0.387332 d), this was judged as an excellent candidate. Nevertheless, the nature of the source remains to be confirmed.

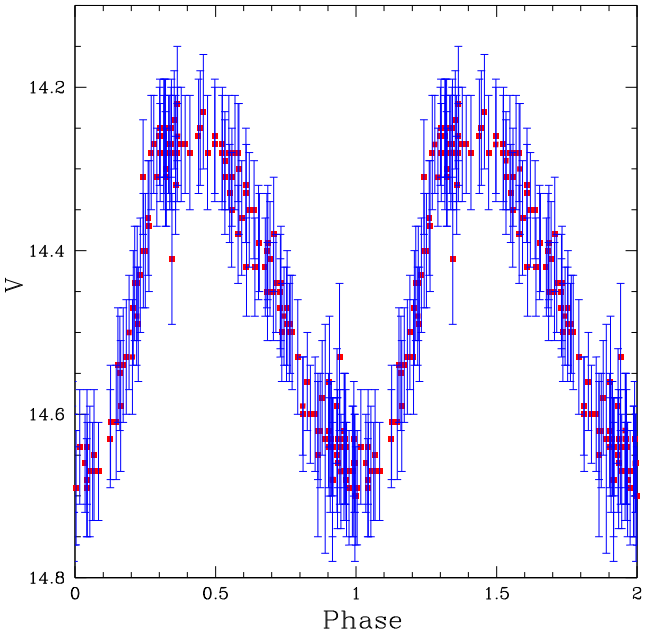

Figure 13. The SSS light curve of AM Oct. The object has a period of ∼0.33 d and is a likely RRc. This object has previously identified as a contact binary in the VSX data base.

6.3 RR Lyrae

RR Lyrae stars are pulsational variables that are often used as standard candles (Catelan 2009, and references therein). In Torrealba et al. (2015), we selected type-ab RR Lyrae from SSS data. These sources provide a means to search for halo structures in areas that are not well covered by other moderately deep wide-field surveys (such as SDSS) that have mainly concentrated on the Northern sky. Our current analysis uses more SSS photometry than Torrealba et al. (2015) and a lower detection threshold. This allows us to find more distant RR Lyrae. Additionally, we also search for type-c RR Lyrae. As demonstrated in DR14, RRc's can be separated from potential confusion with contact binaries when they are well sampled and colour information is available. Thus, these sources can also be used as halo tracers. However, their amplitudes are smaller than RRab's on average, and their absolute magnitudes are not as well studied as those of RRab's. Nevertheless, research is underway to better standardize them (e.g. Kollmeier et al. 2013).

6.3.1 RRc's

RRc variables pulsate in the first radial overtone mode. They have bluer colours and much more sinusoidal light-curve shapes than RRab's (e.g. Catelan & Smith 2015). Since RRc's generally have smaller amplitudes than RRab's, they are more difficult to detect than RRab's of the same brightness. The light curves of poorly sampled, or low-S/N RRc's, can be confused with those of contact binaries. For example, in Fig. 13, we plot the light curve for variable star AM Oct. This object is very likely and RRc variable and is misidentified as contact binary in the General Catalog of Variable Stars (GCVS, Samus et al. 2003), based on Gessner & Meinunger (1974).

As with DR14, we found that the combination of period and $V - W1$ colour was very useful for separating RRc's from contact binaries. Additionally, when phased at their correct periods, RRc's have larger Fourier amplitude (A_1) values (since contact binaries

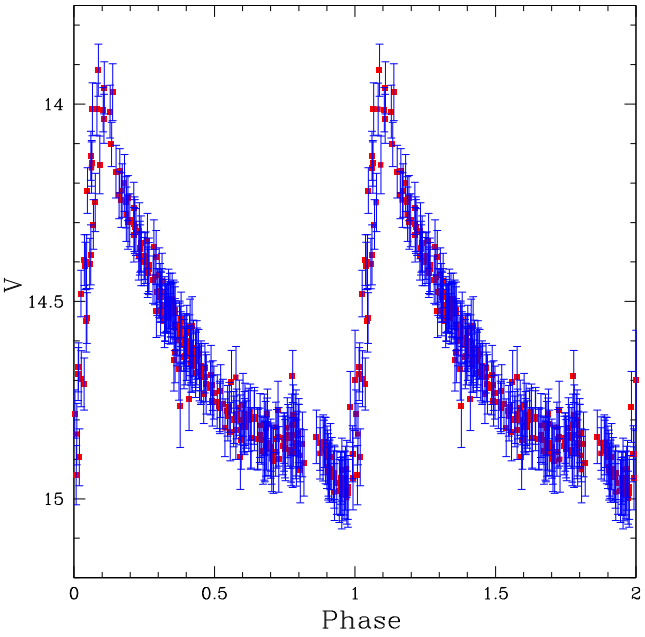

Figure 14. The SSS light curve of AQ Sco. This object is a clear RRab with a period of ∼0.48 d yet is misidentified as an Orion variable in the SIMBAD and VSX data bases, based on Himpel (1944). However, it was correctly identified as an RRab by Samus et al. (2003).

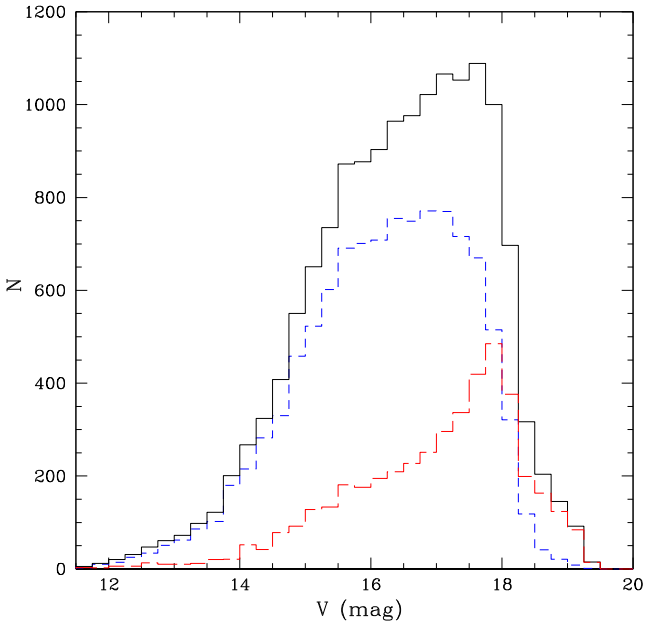

Figure 15. The distribution of SSS RRab magnitudes. The blue short-dashed line shows the distribution from Torrealba et al. (2015). The red long-dashed line shows the new discoveries, and the solid line shows the combined distribution.

exhibit two peaks per period). Lastly, contact binaries generally have smaller M_T values than RRc's. As we have used the same selection process as DR14, where separation was confirmed in that case using SDSS measurements of surface gravity, metallicities, and radial velocities, we expect a low contamination rate. Nevertheless, some misidentifications are likely for longer period EWs, since their colours overlap slightly with RRc's. Overall, we were able to identify ∼4000 RRc's, with magnitudes as faint as $V = 19$.

6.3.2 RRab's

RRab's are fundamental-mode pulsators that have been extensively studied for use both as standard candles and population indicators. In Fig. 14, we present the SSS light curve of known variable AQ Sco detected in this analysis. This RRab is misidentified as an Orion variable by both SIMBAD and VSX data bases, based on Himpel (1944).

In Torrealba et al. (2015), we identified ∼10 500 RRab's in SSS data. Of these ∼9000 were new discoveries. In this analysis, we examined sources using a new $J_{\rm WS}$ variability threshold, a low periodicity threshold, and additional SSS photometry. Together, this has enabled us to identify 4319 additional RRab's. In Fig. 15, we compare the magnitudes of the newly discovered RRab's with those from Torrealba et al. (2015). Clearly our new analysis is mainly finding faint RRab's that were missed during the previous analysis. The peak of the new object distribution is $V_{\rm CSS} \sim 18$, while it was previously $V_{\rm CSS} \sim 17$.

The percentage increase in the number of SSS RRab's identified in this work is similar to the increases in CSS-N RRab's from Drake et al. (2013b) and DR14 compared to Drake et al. (2013a). The combined number from CSS-N, MLS, and SSS data now total ∼33 000 RRab's (including previously known sources).

Many of the new faint RRab's found here are associated with the Sagittarius dwarf (dSph) galaxy stream near the Galactic centre. However, a significant number are also near the Large Magellanic Cloud (LMC). Thousands of RR Lyrae have recently been released in a large region surrounding LMC (Soszyński et al. 2016). Yet no prior surveys have probed the entire region beyond the LMC disc for RR Lyrae. Sources near the LMC were selected for special consideration.

6.3.3 LMC halo RR Lyrae

The main stellar population of the LMC is known to reside in an exponential disc that extends $R \sim 9^\circ$ with a radial scalelength of ∼1.5° (van der Marel 2001). However, recent evidence strongly suggests that the stellar population extends beyond this. For example, Saha et al. (2010) used data obtained with CTIO Blanco 4 m data to trace the LMC's MS stellar population in the range of 7°–19° from the LMC centre. They suggest that the LMC disc is traceable to 16°, although, the existence of an MS population is not clear in fields beyond 14° (their fields F14N and F111). A similar result was also found by Balbinot et al. (2015) using MS stars selected using Dark Energy Survey (DES) data covering a large area of the outer LMC.

Evidence for a kinematically warm component of the LMC stellar halo was initially found by Minniti et al. (2003) and Borissova et al. (2006). However, the Minniti et al. (2003) discovery of a velocity dispersion of $53 \pm 10\,{\rm km\,s^{-1}}$ for LMC RRab's was based on sources in the inner 2.5° of the LMC. In contrast, Majewski et al. (2009) found evidence for a halo extending to 23° from the LMC based on a small number of spectroscopically confirmed red giant branch stars. Similarly, van der Marel & Kallivayalil (2014) found an LMC tidal radius of ∼24° based on *Hubble Space Telescope* data. However, their result also assumed that the LMC rotation curve remains flat at radii well beyond the sources that were actually measured (which were within 10° of the LMC centre) and included a very large uncertainty (∼6°). More recently, Belokurov & Koposov (2016) found evidence for overdensities of candidate blue horizontal branch (BHB) stars extending 30°–50° from the LMC and also discovered

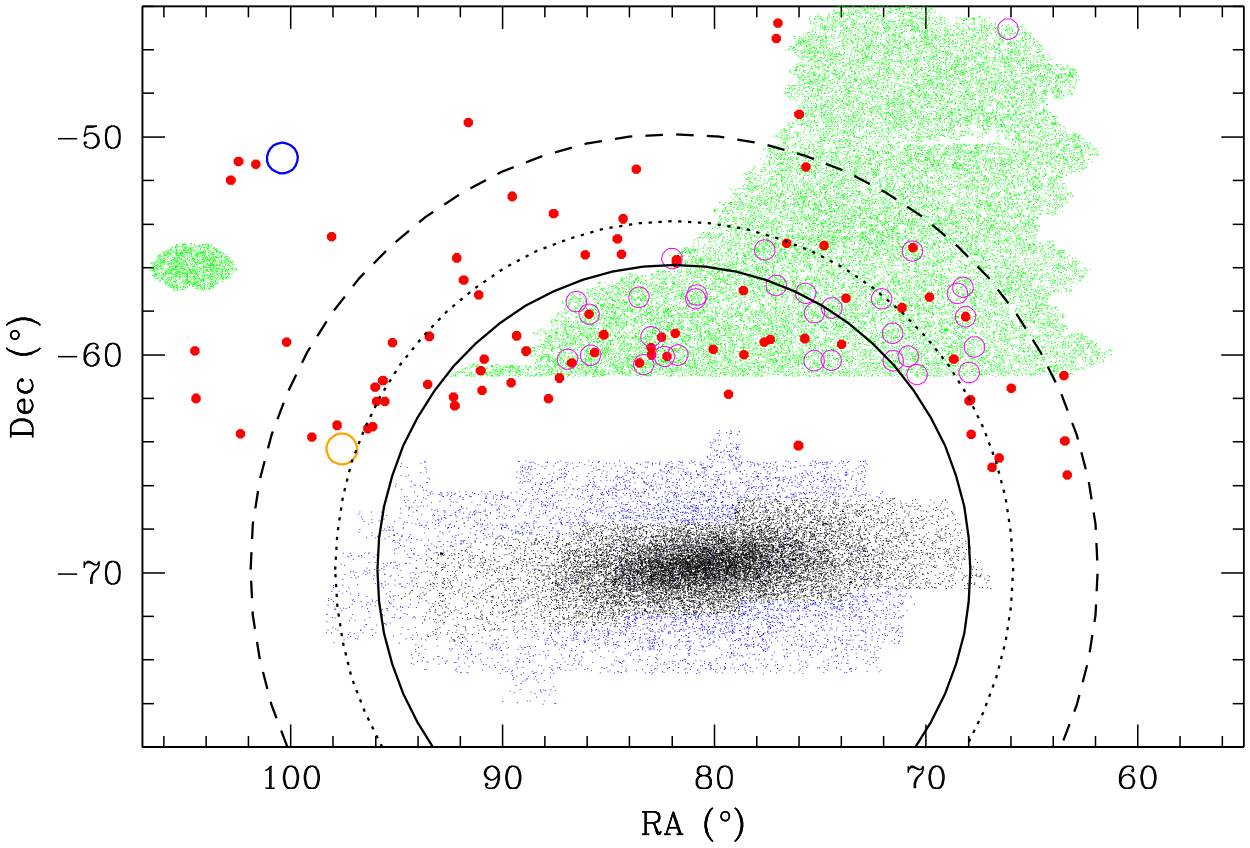

Figure 16. The distribution of LMC RRab's. The black points give the location of 17 693 LMC RRab's discovered by OGLE-III (Soszyński et al. 2009) and 5778 LMC RRab's from the EROS-II (Kim et al. 2014) survey. The large red dots are likely LMC-associated RRab's from this work. The green points are the location of DES sources with colours and magnitudes consistent with LMC RRab's. The large magenta circles are the locations where additional RRab's were discovered based on DES photometry. The three large circles give 14°, 16°, and 20° radii from the LMC centre location based on van der Marel et al. (2002). The large orange circle shows the location of the globular cluster NGC 1841. The large blue circle shows the location of the Carina dSph galaxy.

evidence for the long-sought-after population of stars associated with the Magellanic Bridge.

In Fig. 16, we show the locations of SSS RRab's that are consistent with the distance to the LMC ($40 < d$[kpc] < 60). These RRab's are clearly seen to surround the LMC, yet extend more than 20° from its centre. Comparing the number of distant RRab's near the LMC with those in the same spatial volume in other regions away from the LMC (and the Sagittarius dSph tidal stream), there is no doubt that the overdensity of these sources far exceeds the halo density. We note that the RR Lyrae locations do not match the positions of the known outer halo LMC globular cluster NGC 1841, nor the Carina dSph galaxy. This analysis confirms the preliminary findings we presented in Drake et al. (2016). That is, we find evidence for the presence of an old stellar halo extending to at least 20° from the centre of the LMC. In Fig. 17, we provide examples of the light curves for the faint LMC RRab's.

Our current analysis does not reveal a sufficient number of LMC RRab's to confirm that the LMC stellar halo extends as far 30°–50° as suggested by Belokurov & Koposov (2016). However, we note that there remains some uncertainty in that result, since BHB candidates selected based on colour are often contaminated by foreground young MS stars and halo blue stragglers (Momany et al. 2007). In particular, the lack of any *u*-band observations from DES almost certainly introduces contamination of the BHB candidates by QSOs and WDs. Unlike BHB candidates, additional deep spectroscopic observations are only required to confirm the nature of RRab candidates when they do not have well-defined light curves.

An alternative explanation for the distant RRab's that we find is that they may be associated with a tidal feature. Mackey et al. (2016) found evidence for a stream-like structure extending between 9° and 12° from the LMC centre, based on photometrically selected MS turnoff stars. However, the RRab's are sparse and not thus ideal for tracing the inner region where these structures were observed.

The detection efficiency tests performed by Torrealba et al. (2015) suggest that our RRab detection efficiency is only ∼10 per cent at the distance of the LMC. A much larger population of LMC RRab's is almost certainly present in these regions. Indeed, many of the RRab's discovered by Kim et al. (2014) in EROS-II data are more than 16° from the LMC centre, yet are not detected by our survey due to their low luminosity, combined with the small number of observations and crowding. However, in the outer LMC fields there is no crowding and there are more observations [the Small Magellanic Cloud (SMC) and LMC themselves are avoided due to crowding]. This suggested the possibility of increasing the RRab detection efficiency by combining SSS with deeper data. In Appendix A, we present details of our search for additional halo RRab's utilizing public DES data.

In this paper, we have not attempted to associate the distant RRab's into potential sub-structures due to the relatively small number of sources. Surveys such as *Gaia* have started to reveal halo RRab's in the Southern sky (Clementini et al. 2016) and thus provide a means for testing the validity of the halo galaxy candidates given by Belokurov & Koposov (2016). For example, during the preparation of this paper Belokurov et al. (2017) used *Gaia* data

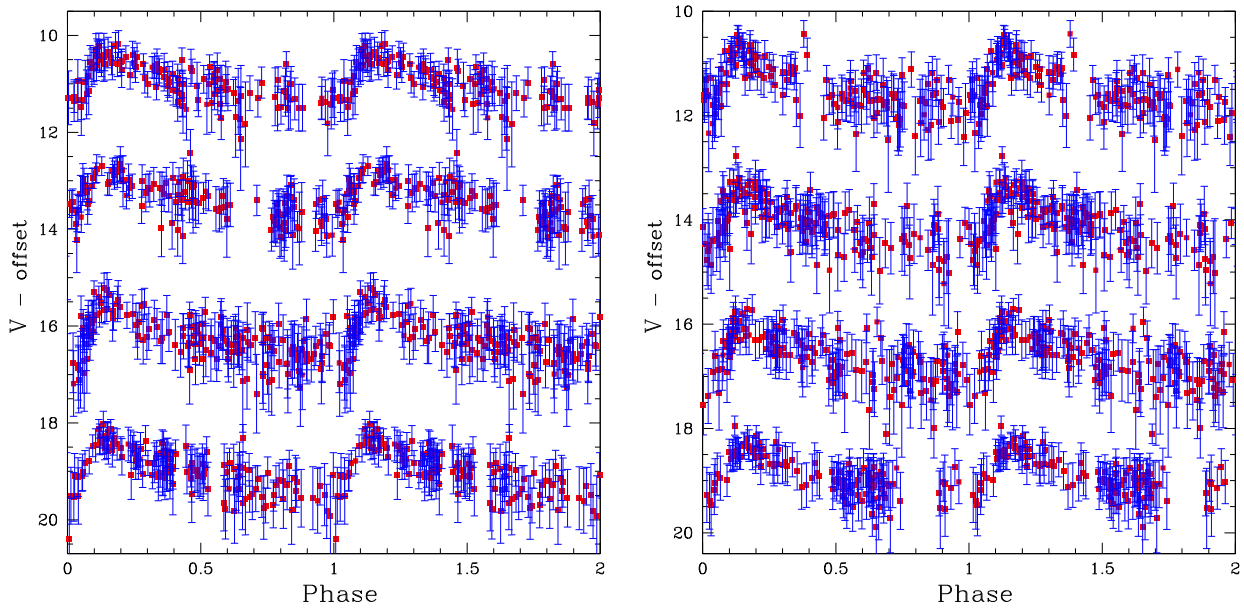

Figure 17. Examples of SSS light curves of LMC RRab stars. In the right-hand panel, from bottom to top, these are: SSSJ060352.9−613738 (0.504 d), SSSJ054423.1−552428 (0.529 d), SSSJ063601.8−634558 (0.642 d), and SSSJ055532.5−594940 (0.614 d). Here, the top three light curves have been offset by 3, 5.5, and 8 mag to avoid confusion due to overlap. In the left-hand panel, from bottom to top, these are: SSSJ050925.9−591749 (0.573 d), SSSJ053734.0−552231 (0.588 d), SSSJ065756.6−620002 (0.563 d), and SSSJ053149.1−600014 (0.524 d). Here, the top three light curves have been offset by 2.5, 5, and 7.5 mag to avoid confusion due to overlap.

to select candidates variables with RR Lyrae colours surrounding both MCs. In the near future sufficient *Gaia* data should be available to clearly select the RRab's from among the Belokurov et al. (2017) candidates.

6.3.4 RRd's and Blazhko RR Lyrae

Apart from single-mode, fundamental or first overtone pulsations, RR Lyrae are also known to exhibit multimodal variations. Type-d RR Lyrae (RRd's) simultaneously oscillate in both the fundamental and first overtone modes. The phased light curves of RRd's often resemble those of RRc's where the determined period is slight incorrectly. However, this possibility can generally be ruled out for objects that have been observed hundreds of times. The presence of an additional frequency is generally established via Fourier analysis detection. A period ratio near ∼0.745 is typically observed (Alcock et al. 1996; Catelan & Smith 2015, and references therein).

In contrast to RRd's, Blazhko RR Lyrae exhibit a modulation in amplitude and phase. When phase-folded over many cycles their light curves often appear like those of RRab's where the phase of the peak brightness varies. In Fig. 18, we plot the light curve of a candidate RR Lyrae with a moderate Blazhko effect.

These two types of RR Lyrae can be distinguished, since RRd have dominant periods and colours similar to RRc's, while most Blazhko RR Lyrae have periods and colours close to RRab's. Nevertheless, a small number of RRc's and a large fraction of RRd's have recently been found to exhibit the Blazhko effect (Wils, Kleidis & Broens 2008; Jurcsik et al. 2014, 2015). It is also possible to confuse genuine such objects with those having incorrectly determined periods. Thus, further investigation of these sources is warranted.

6.4 Type-II Cepheids

Cep-II are metal-poor pulsators that are found in galaxy haloes. These stars can be distinguished from Classical Cepheids by their

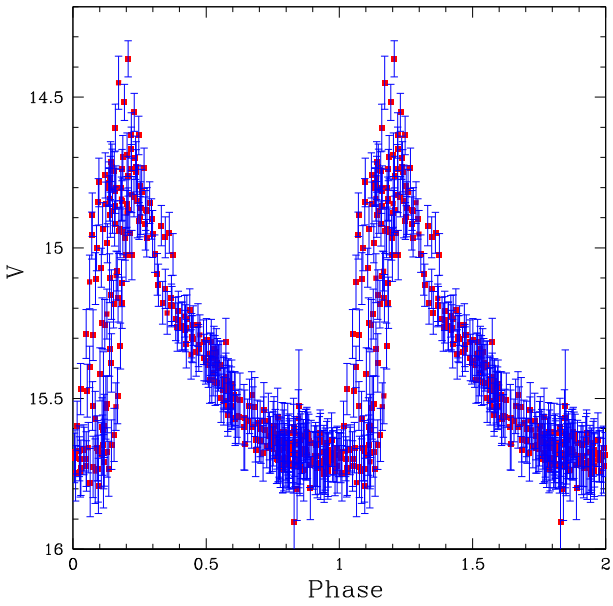

Figure 18. The SSS light curve of likely Blazhko RR Lyrae SSSJ143242.7−282136 phased with a period of ∼0.489 d. Slight variations in the phase and magnitude like this are often seen in RR Lyrae due to the Blazhko effect. However, most Blazhko RR Lyrae appear more random than this in SSS data, since they were observed over thousands of days.

amplitudes, light curves, spectral characteristics, and radial velocity curves. They are fainter than Classical Cepheids and are often divided into three sub-classes that are separated by increasing period and luminosity, for example, as noted by Wallerstein (2002). They are also thought to be the progeny of BHB stars (Catelan & Smith 2015, and references therein).

The proposed sub-classes include BL Herculis variables (BL Her), with periods between 1 and 5 d; W Virginis variables

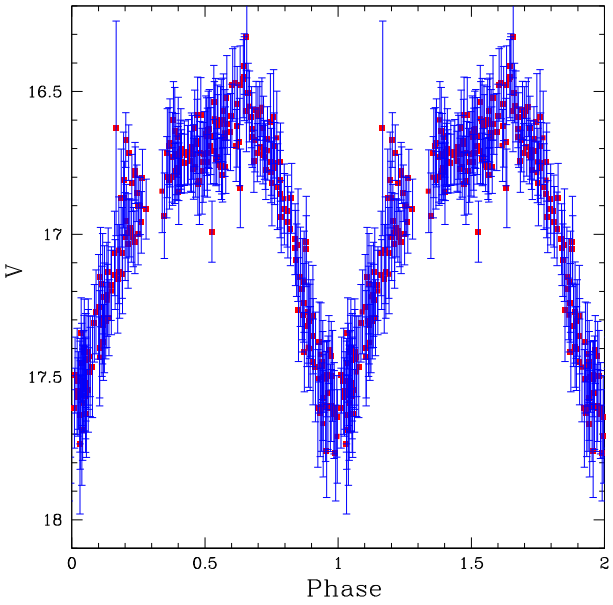

Figure 19. The SSS light curves of BL Her Cepheid SSSJ234924.7−392630 having a period of ∼0.92 d.

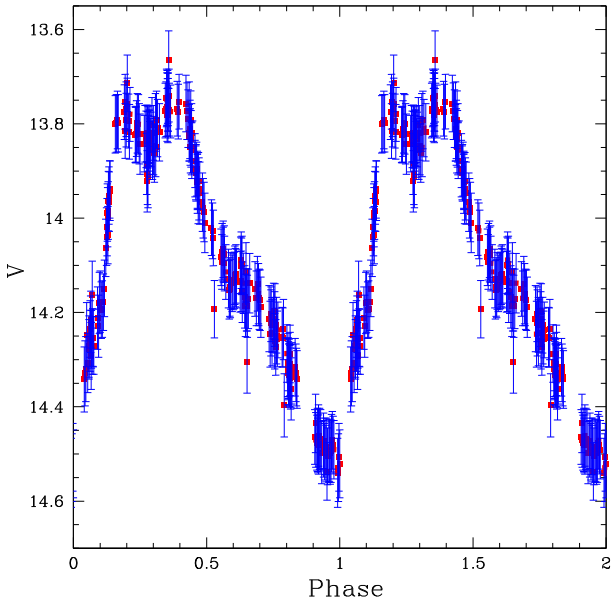

Figure 20. The SSS light curves of Anomalous Cepheid SSSJ124606.5−423805 having a period of ∼2.92 d.

(W Vir) with periods of 5–20 d; and RV-Tauri variables (RV Tau), with periods greater than 20 d. However, as recently reviewed in Catelan & Smith (2015), the exact periods used for dividing types remain the subject of much debate. Nevertheless, like Classical Cepheids, these variables can be useful for measuring distances since they too obey a period–luminosity relationship (e.g. McNamara 1995; Pritzl et al. 2003; Soszyński et al. 2008).

6.4.1 Anomalous Cepheids and BL Her stars

As in DR14, we discovered many sources with RRab-like light curves that had much longer periods and larger amplitudes than RRab's. Additionally, within the period range of RRab's we also identified sources with very different, rounder light curves than RRab's that include significant humps. These objects are a combination of Classical Cepheids, Anomalous Cepheids, and BL Hers.

BL Her-type Cepheids are Cep-II that usually show a bump on the descending side of their light curves for short-period sources, and on the ascending side at longer periods (Soszyński et al. 2008). BL Hers have similar spectral types to RR Lyrae, but are known to be slightly brighter. BL Hers with periods between 1 and 3 d are referred to as 'above the horizontal branch' stars (AHB1) by some authors (e.g. Sandage & Tammann 2006), since BL Her itself has a near-solar metallicity and has been judged as unrepresentative of the group of metal-poor Cep-II.

Anomalous Cepheids (ACs) have periods that overlap with BL Hers and Classical Cepheids, but have so far generally been discovered in dwarf galaxies and (to a much smaller extent) globular clusters (Catelan & Smith 2015, and references therein). Division of ACs and BL Hers is difficult for field stars due to the mixture of stellar populations in the field and the lack of well-defined distances.

In this analysis, we chose to divide these variables into objects with RRab-like light curves, yet much larger amplitudes than RRab's at their given periods (which ranged from 0.71 to 4.6 d), and those with bumps and other features in their light curves. In Fig. 19, we plot the light curve of one of the sources placed in the BL Her class, while Fig. 20 shows an example with a clear bump.

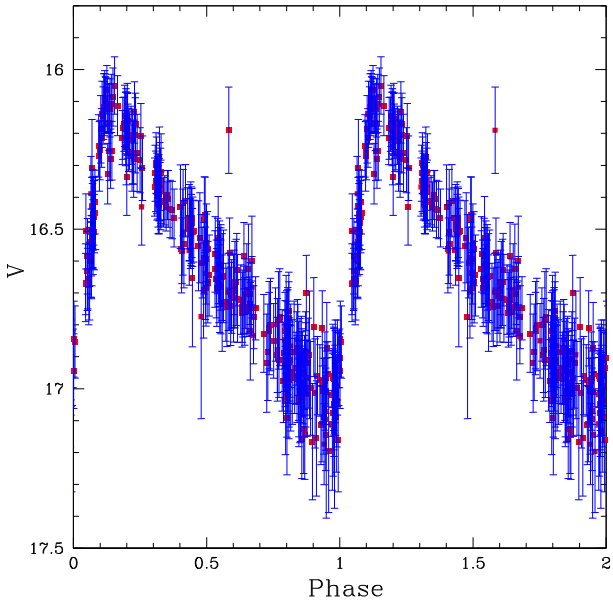

Figure 21. The SSS light curve of LMC Classical Cepheid SSSJ105538.4−302137 having a period of ∼1.89 d.

The RRab-like objects are a mixture of Classical Cepheids and Anomalous Cepheids. As shown by Soszyński et al. (2015), the division between these two types of Cepheids is very slight. Without knowledge of the distance (as is the case of LMC or globular cluster sources), this division is hard to discern. We found 10 Cepheids that clearly had luminosities based on their periods that were consistent with membership of the LMC. Only one of these was previously known (SSS_J043856.8−694118 = OGLE LMC150.6 5206). Two of the sources are far from the centre of the LMC (SSS_J052440.3−555907 and SSS_J042026.5−575104), yet have derived distances, periods and light curves consistent with them being LMC sources. In Fig. 21, we plot an example light curve of one of the LMC Classical Cepheids we discovered.

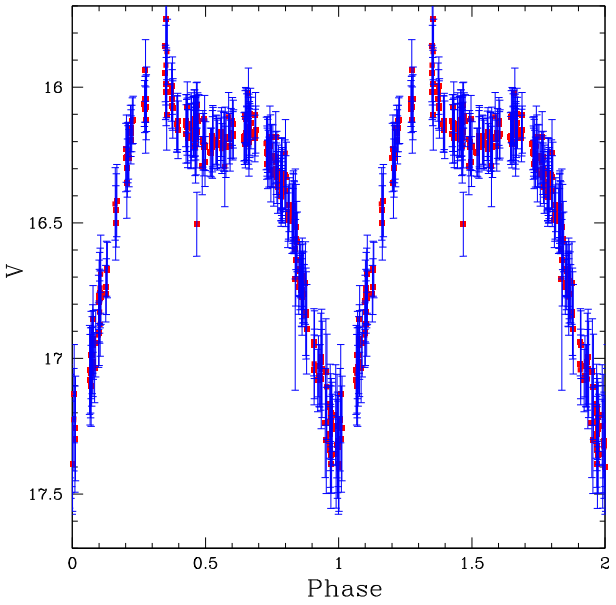

Figure 22. The SSS light curves of W Vir type Cepheid SSSJ091832.2−274627 with a period of ∼5.24 d.

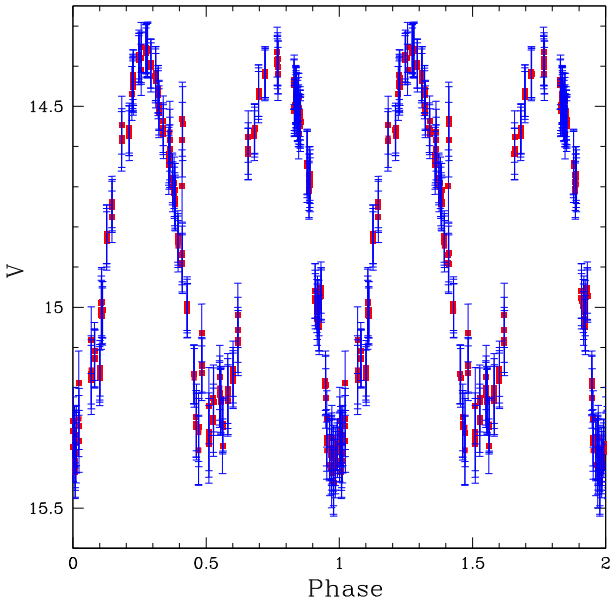

Figure 23. The SSS light curves of SS Mic, and RV-Tau variable with a period of ∼32.25 d. This object was previously noted as an RR Lyrae in SIMBAD.

A number of the other RRab-like sources have brighter magnitudes consistent with them being Galactic Classical Cepheids. However, it is not possible to unambiguously determine whether these are Classical Cepheids or Anomalous Cepheids from their light curves. However, the sources with the shortest periods ($P < 1.6$ d) are more likely to be ACs since short periods are not observed in the Galactic Classical Cepheid population. Therefore, we only divide the RRab-like sources into LMC Classical Cepheids and other Cepheids. Further work with Fourier decomposition and spectroscopic follow-up is necessary to gain a better idea of the origin and classification of these sources.

6.4.2 W Vir and RV-Tau Cepheids

W Vir is the archetype for Cep-II. This star has a period of 17 d. Stars of the W Vir sub-type have periods longer than ∼5 d and do not exhibit the bumps that are sometimes present in BL Her stars. In contrast, RV-Tau-type Cepheids exhibit a secondary dip with distinctive alternating deep and shallow minima. However, the light-curve morphology varies greatly among Cep-II of similar period. This may be linked to differences in metallicity. In Figs 22 and 23, we plot examples of W Vir and RV-Tau-type light curves.

6.5 δ Scutis

δ Scuti variables are pulsators that exhibit brightness variations between 0.001 and 1.7 mag (in V), and have periods of a few minutes to several hours. These stars can exhibit large numbers of simultaneous oscillation modes (Breger et al. 2005; Catelan & Smith 2015, and references therein). Generally, δ Scutis are divided into two groups: high-amplitude δ Scutis (HADS, or AI Velorum stars: Bessell 1969) with amplitudes greater than ∼0.1 mag (Alcock et al. 2000), and low-amplitude δ Scutis (LADS) with smaller amplitudes. In Fig. 24, we plot an example of a HADS.

In our analysis, we are mainly sensitive to those δ Scuti with variations >0.1 mag and periods of hours where a single pulsation mode dominates. Since, in addition, HADS may represent but a small fraction of the total number of δ Scutis (Lee et al. 2008), it is likely that we have only detected a small fraction of the δ Scutis in our fields.

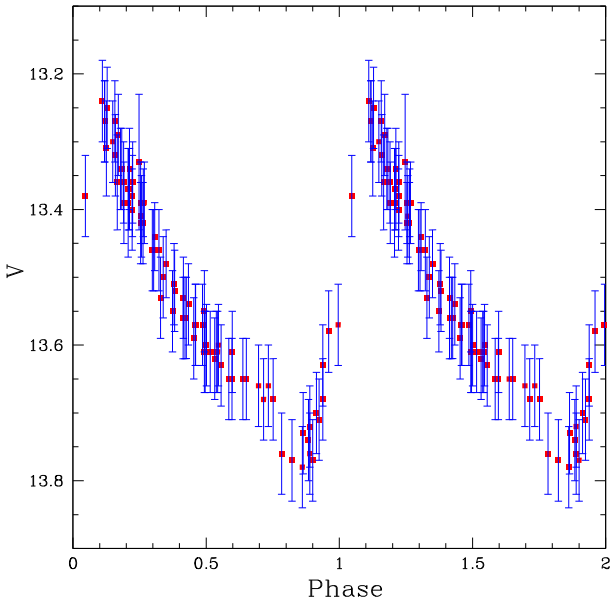

Figure 24. The SSS light curve of LP Car. The source is a clear high-amplitude δ Scuti star with a period of ∼0.22 d, and was previously identified as an RR Lyrae variable in SIMBAD based on Gavrilchenko et al. (2014).

6.6 Rotational variables

RS CVn's consist of spotted stars in binaries with periods from <1 d to hundreds of days (Drake 2006). The groups of spots typically give rise to periodic variations with amplitudes of ∼0.2 mag. However, the numbers, sizes, and locations of spots are often seen to change over time. This leads to changes in the phase and amplitude of the variations. Ellipsiodal variables also vary with stellar rotation.

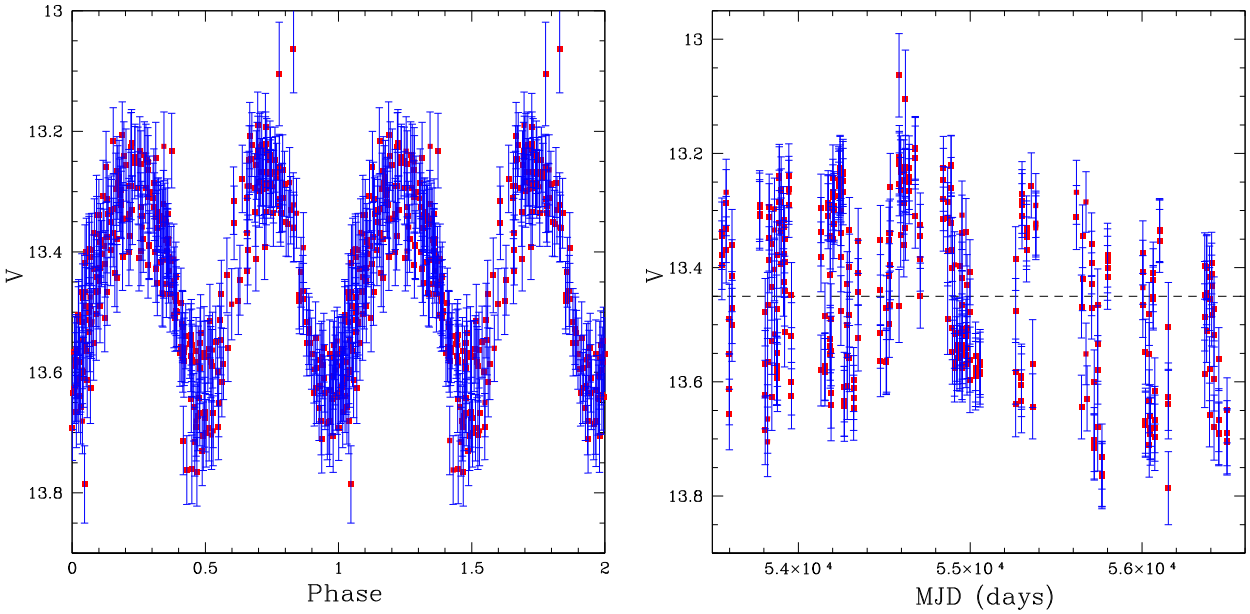

Figure 25. The SSS light curve of spotted eclipsing variable star SSSJ141205.8−365502. The left-hand panel shows the light curve phased with period ∼0.33 d, while the right-hand panel shows the unphased SSS data.

In Fig. 25, we show the raw and phased light curve of a spotted variable system. The average brightness of the sources varies significantly as the degree spot coverage changes. In addition, the variations suggest that this particular system is also a contact binary.

6.7 Long-period variables

LPVs are cool pulsating giants with periods ranging from a few to over a thousand days. The amplitudes and shape of the magnitude variations in LPV light curves can vary greatly, and so they are frequently sub-divided into Mira, semiregular, and irregular subtypes (Catelan & Smith 2015, and references therein). Due to these variations, for the SSS LPVs, the scatter in the phased light curve is greater than the actual photometric uncertainty. In Fig. 26, we plot an example of an LPV light curve.

As shown in DR14, LPVs with apparently faint magnitudes lie within the Galactic halo. Like RR Lyrae stars, these can be used to trace halo streams and the presence of dwarf galaxies (Huxor & Grebel 2015). Since LPVs are intrinsically much brighter than RR Lyrae, and often have much larger amplitudes as well, they can be used to detect much more distant halo features. However, they are also far less common than RR Lyrae. Thus, the detection of multiple LPVs associated with a faint dwarf galaxy is less likely.

To investigate whether any of the faint LPVs we found were associated with nearby dwarf galaxies, we selected the 44 faint LPVs with median magnitude $V > 16$ from the full SSS sample of ∼1000. Among these, nine had median magnitudes of approximately $V = 17$ and had been previously associated with the Fornax dSph. Two of these LPVs were clearly associated with the Sculptor dSph, one matched the location of the Carina dSph, another matched the SMC, and one was found to be on the outskirts of the LMC globular cluster NGC 2257. Of the remaining LPVs, no clear associations to known Milky Way dwarf galaxy satellites were found. It is possible that some of these remaining objects are associated with distant faint dwarf galaxies or streams that are yet to be detected.

Among the brighter LPVs, approximately 70 had median magnitudes of $V \sim 15.5$, and locations consistent with the LMC. These objects were overall closer to the LMC centre than the LMC RRab's we investigated earlier, and thus are more unlikely to be associated with the LMC halo. Approximately 50 of the LPVs were clumped near the Galactic bulge. These have median magnitudes of ∼14.2 and are clearly associated with the Sagittarius dSph galaxy.

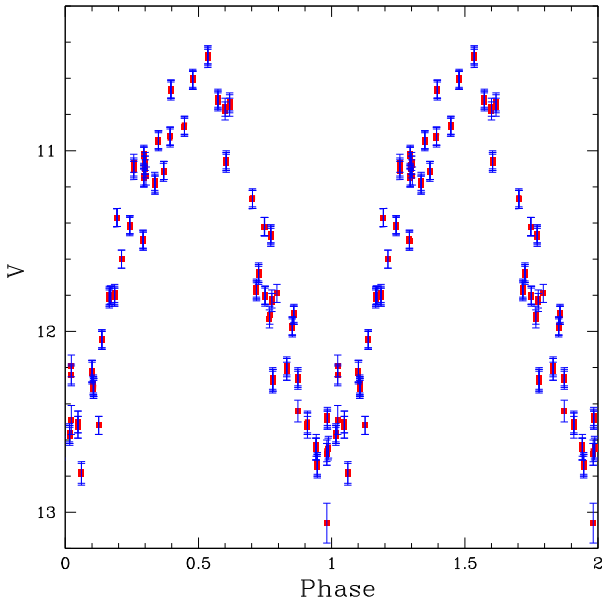

Figure 26. The SSS light curve of V2064 Oph. The source is clearly an LPV since it has a period of ∼246 d. Like most LPV, there are moderate variations between cycles that introduce scatter into the phased light curve and lead to uncertainties in the determined periods. This object was previously identified as being an Orion-type variable.

6.8 Miscellaneous variable sources

More than 99 per cent of the periodic variables that we inspected clearly fell into one of the main variable star groups described above.

However, some of the periodic variables were difficult to classify. In many cases, this is because there was more than one kind of variability present –for example objects that are both eclipsing binaries and spotted variables. Our inspection also led to the discovery of a number of periodic sources where the light curve did not fit any of the existing classifications. All of these sources were placed in the miscellaneous category along with the compact binaries (as noted above).

Additionally, as with DR14, we detected many highly variable sources with no clear periodicity. Many are simply irregular variable stars and QSOs. In some cases, these objects exhibited large outbursts and had moderately bright UV detections in *GALEX* data. These objects are generally dwarf novae-type CVs. Details of these sources are given in Appendix B.

7 COMPLETENESS, ACCURACY, AND PURITY

Three possible ways of measuring the utility of an astronomical source catalogue are its purity, accuracy, and completeness. The natural expectation is that a periodic variable star catalogue should consist purely of stellar sources. Additionally, such a catalogue should provide accurate periods, magnitudes, amplitudes, and classifications. One might also naturally expect the level of completeness to be least equivalent to prior catalogues covering the same region of the sky.

In the DR14 catalogue, we discovered that some source misclassifications occurred based on our comparison of the catalogue with spectroscopically classified QSOs and galaxies. Here, we expect a slightly higher rate of misclassification due to the current lack of a Southern equivalent to the multiband optical photometry and spectra provided by SDSS. This situation should be improved in the near future when Southern surveys (such as DES, LSST, and *Gaia*) provide deep multicolour photometry of these sources.

7.1 Completeness

The International VSX (Watson 2006) provides what is likely the most complete catalogue of known variable stars. Similarly, SIMBAD (Wenger et al. 2000) provides information for millions of astronomical sources, including detailed citation and bibliographic references for very large numbers of periodic variable stars.

We cross-matched our initial ∼270 000 periodic variable candidates with both VSX and SIMBAD using a 5″ matching radius. We found 13 472 matches to VSX sources, of which 12 866 had periods associated with them. However, a very large fraction of the VSX matches (9079) were RR Lyrae that we had previously discovered and published in Torrealba et al. (2015). Note that the number is less than the full SSS RRab catalogue since that work was not limited to the region $\delta < -20^{\circ}$. The number of matches from other sources is thus only ∼ 3800.

Our cross-match with SIMBAD sources gave 15 259 matches. However, in this case, approximately 5000 of the matches we found were related to galaxies [active galactic nucleus (AGN) and QSO], and another ∼5000 were simply marked as 'Stars'. The remaining matches contained both variable stars and other types of objects (e.g. X-ray and radio sources, and high proper motion stars).

In order to determine how complete our periodic selection process was, we decided to compare how many of the initial matches remained in our final periodic variable catalogue. VSX sources that matched our initial candidates but were missing from our final periodic variable catalogue include aperiodic objects such as CK Eri, a clear CV that is classified as an RR Lyrae in the GCVS and VSX, based on Hoffmeister (1963).

However, we found that 986 VSX matches with periods among our initial candidates did not have matches in our final catalogue, while 2859 did. Initially, this seemed to suggest a large fraction of the periodic sources had been missed. Investigating further, we discovered that 577 of these sources were marked in VSX as 'MISC' type. Most of these originated from the ASAS survey (Pojmanski 2002). This class is noted by VSX as including red variables, such as semiregular variables and irregular variables. Reviewing the light curves, we discovered that most of these sources did not exhibit evidence for periods matching those given by VSX. These sources were clearly variable, but irregular. Approximately 250 of the missing periodic matches were bright semiregular or Mira variables. We found most of these were saturated since our data are much deeper than ASAS. Another ∼50 of the sources are classified as possible eclipsing binaries by VSX. For many of the sources, we found no evidence for periodicity based on our inspection of the SSS data. However, some were genuine periodic variables that we had missed.

Of the remaining missing VSX sources, only 19 were marked as RR Lyrae. Among these, six had been given multiple classifications, since their true nature was apparently uncertain. Approximately 100 of the missing periodic sources are classified as CVs. In most cases, the periods given by VSX are based on detailed follow-up of the modulations during outbursts (although a small number are orbital periods based on eclipses). The SSS data are too sparse to detect such outburst modulations. Considering the saturated, aperiodic, and rapidly varying systems, only ∼100 of the missing VSX matches could have been detected in the SSS data.

Carrying out the same process with the SIMBAD matches, we found 11 369 sources that did not match our periodic source catalogue. After removing the objects that are simply classified as 'Star', this reduces to 7259 missing sources. 5039 of these sources are classified as galaxies, QSOs and AGN, whose removal validates that our selection has removed a very large fraction of the aperiodic variable sources. Apart from these, 35 of the missing SIMBAD matches are classified as RR Lyrae and 54 as eclipsing binaries. The remaining missing matches had SIMBAD classifications as high proper motion stars, radio sources, stars within clusters, and horizontal branch (HB) stars. Among these, only the HB stars are expected to include some fraction of periodic variables. These 61 missing SIMBAD HB candidates were among 606 that initially had matches. These sources are predominately from Christlieb et al. (2005), who note that <16 per cent of their sample may represent MS A-stars contaminants. Examining the sources, we found some had moderately blue NUV $-$ $V_{\rm CSS}$ colours based on *GALEX* UV data. This suggests that many of these are QSOs or WDs, rather than HB stars. Other HB candidates had no discernible periodicity. These are most likely a combination of MS A-stars, low-amplitude RR Lyrae, WDs, and other non-variable stars. In total, less than 100 of the initial candidates with SIMBAD matches that appear to be genuine periodic variables were found not to be in our final catalogue.

Overall, the comparisons with VSX and SIMBAD suggest that a small percentage of genuine periodic variables were missed during the classification process. The largest group of known missing periodic variables were red giant variables that are saturated in the SSS data. However, the truly largest group of missing periodic sources is likely to be those objects that were not selected among our initial 270 000 periodic variable candidates. Such objects could have been missed due to poor coverage, bad data, as well as periods, amplitudes, and luminosities fainter than our sensitivity limits.

Table 5. Catalina variables with VSX matches. The first row gives the class of periodic variable from the current analysis, and the first column gives the classes based on the VSX. Here, the VSX variability types have been combined to match our classifications as follows: (E, EA, ED, EB, ESD) = EA; (EC, EW) = EW; (AHB1, CWB, CWA, CW) = ACEP; DCEP = CEP; (RRAB, RR) = RRab; (DSCT, HADS) = δ Scuti; (LPV, M, SR, SRA, SRD, RVA) = LPV; (MISC, SXPHE, VAR, BY, etc.) = Misc. Note, for objects simply marked an RR (RR Lyrae) in VSX, we take this to match our RR Lyrae sub-type even though this is not specified.

Type	EA	EW	CEP	ACEP	DS	LPV	RRab	RRc	RRd	Blazhko	ROT	Misc
EA	272	113		1							2	1
EW	3	749		2				11	2		37	4
CEP		1	5				1				1	
ACEP			9	12		1	1					
DS		22			13			1			1	
LPV				2		367						
RRab	1	6	19				141	13	51		3	2
RRc		15					3	153	36	3	9	
RRd		1					1	1	18	2	1	1
Blazhko												
ROT											2	
Misc		7		3	1	31	1	1	0	2	13	2

Since the completeness of VSX and SIMBAD catalogues themselves is not known (due to the highly heterogeneous nature of underlying observations), we can only estimate the completeness of our catalogue based on the number of matches and the thousands of periodic variables that we found in addition to those in the VSX and SIMBAD data bases.

7.2 Accuracy and purity

After having investigated the variable sources that were in our initial selection, yet not amongst the catalogue of periodic variables, we decided to compare the classifications of the sources with matches. Ideally this test should enable us to determine the level of agreement, and thus the approximate accuracy of the classifications. However, this is only possible if the comparison set itself purely consists of the objects specified.

7.2.1 SIMBAD

We found 1595 SIMBAD matches to our catalogue sources after removing objects that were simply classified as 'Star'. Investigating the SIMBAD sources that were marked as RR Lyrae, we found that many were incorrectly classified. A large fraction of the misclassifications referenced Gavrilchenko et al. (2014), who had gathered lists of sources previously classified as RR Lyrae with the aim of producing mid-IR templates for RR Lyrae. One example of these incorrectly classified variable stars is BS Hya. This object is noted in Gavrilchenko et al. (2014) among 3740 'good' RR Lyrae candidates. However, it is undoubtedly an eclipsing binary, based on SSS data. Nevertheless, the number of matches between our catalogue and those of Gavrilchenko et al. (2014) is only a fraction of the objects in these catalogues.

In the classification context, it is worth noting that the β Lyrae variable VY Dor (noted earlier, Fig. 10), was specifically included in the catalogue of 'properly identified' RR Lyrae brighter than V=12.5 by Maintz (2005). This variable system is also included in the 3740 'good' RR Lyrae of Gavrilchenko et al. (2014). Additional misidentifications of named variable stars include LP Car (noted above, Fig. 24), a δ Scuti; EQ Lib, an LPV; and V447 Cen, KK Hya, ZZ Phe, CH Pav, and V2215 Sgr, all contact binaries.

In additional to these sources, we also found many other periodic variable stars that were noted as QSO candidates in SIMBAD based on Atlee & Gould (2007). Furthermore, in a small number of cases we found that periodic variables in our catalogue were classified as galaxies within the SIMBAD data base. For example, both LCRS B214338.3−454633 and LARCS a3888r24−1545 are periodic variables rather than galaxies. In some cases, these periodic variable stars were found to be blended with a galaxy (e.g. APMBGC 342+001-073), or misclassified as a galaxy due to the poor quality of the spectra used for their classification (e.g. 6dFGS gJ130606.2−281608). The presence of misidentified sources in SIMBAD is not surprising given the highly heterogeneous nature of the data. In part, the cause is likely that many GCVS variables were identified long ago without the aid of modern instrumentation.

Given the large number of misidentifications, we do not believe that a comparison between our catalogue and SIMBAD can provide more than a qualitative test of our classification accuracy.

7.2.2 VSX

Comparing our variable star catalogue with VSX, we found 3193 of the 37 745 sources in our catalogue had matches. The VSX catalogue provides periods for 2859 of these. The VSX classifications appear to be more accurate than SIMBAD's, yet still contain some incorrect entries. Among the objects with matches to VSX, 614 sources have been given multiple classifications by VSX. Inspecting the light curves of many of these sources, we found that the reason appeared to be mainly an uncertain classification, rather than the presence of multiple types of variability. The remaining 2245 sources with a VSX period and single variability type were chosen as the best sample for comparing variability classifications.

In Table 5, we compare the classifications given by VSX with those we determined in our analysis. As VSX contains many more variability categories (which in some cases overlap others due to differences in the notation used by surveys) than our analysis, we condensed the VSX categories into the more general types that we had used. For example, we include the contact and semidetached binaries in the same group in our analysis.

Overall the agreement between the two sets of classifications is good. In particular, most sources that we classify as eclipsing binaries, RR Lyrae, and LPVs are classified the same way by VSX.

One difference occurs with the objects that we have classified as Blazhko RR Lyrae. None of these stars is classified as a Blazhko

RR Lyrae by VSX, where they appear instead, for the most part, simply as RRab stars.

Likewise, very few of the objects that we classify as RRd's are classified in this way by VSX. This is the case even when VSX presents objects classified based on our public SSS data. We do not believe that the stars we identified as RRd's are all oscillating with a single frequency, as in the case of RRab's and RRc's, so we can only conclude that VSX has cautiously classified these sources as other types until further analysis has been undertaken to prove the classifications – for example checking for the presence of multiple frequencies and amplitudes using Fourier analysis.

In the VSX, many of the sources that we classify as contact binaries are instead labelled as detached and semidetached systems. Since we did not try to distinguish semidetached systems from contact systems (due to the similarity of their light curves), some amount of disagreement is natural. As expected, most of the systems where there was a different type of binary classification were noted as semidetached systems in VSX.

Most of the VSX sources that we classify as spotted or ellipsoidal variables are noted as contact binaries by VSX. These types of variable stars generally have smaller amplitudes than contact binaries, and unlike most contact binaries, often have asymmetric shapes. Furthermore, contact binaries without spots do not exhibit significant changes in light-curve shape with time. Nevertheless, most have light curves that are close to sinusoidal, so it is often hard to distinguish the two types based on their light curves alone. Radial velocity measurements would give a definitive answer in most cases.

Another source of confusion is the similarity of the light curves of contact binaries and RRc's. However, the $V_{\rm CSS} - W1$ colours of these variables are significantly different in most cases. Thus, as expected there were some differences in the RRc and contact binary classifications. Eleven of the sources that we had classified as RRc's were noted as contact binaries in VSX, and 15 of the sources we classified as contact binaries were classified as RRc's by VSX. After reviewing the light curves and colours of all these objects, we did not change our classifications.

One of the most common causes of an incorrect classification is a poorly determined period. For example, like SIMBAD, VSX also notes BS Hya as an RRab. However, VSX provides a period of 0.44775 d. From our data, we see that this eclipsing binary actually has a period of 0.5551 d. Similarly, SSS_J101745.3−291636 is noted by VSX as a W Vir (Cep-II) with a period of 1.00272 d (based on our public SSS data). However, the SSS light curve clearly shows that this object is an LPV (with a period of ∼368 d). The one day period presented by VSX is clearly due to a sampling alias. We also found a few cases where we had misclassified the type of variability based on an incorrect period. We have corrected the classifications and periods for those sources.

Based on the fraction of VSX matches with incorrect periods, we expect that there are at least 100 variables in the catalogue with an incorrect period. Nevertheless, differences in classification are not always due to poor period determination. For example, the previously known variable KK Hya is noted by VSX as an RRab with period 0.41141 d. Although this period is correct, the light curve (presented earlier in Fig. 8) shows that this object is definitely not an RRab, but rather an eclipsing binary presenting the O'Connell effect.

Overall, the presence of many misclassified objects shows that neither SIMBAD nor VSX can be considered the ground truth for classification purposes. This point is very important to consider when investigating the completeness and accuracy for both human and automated classifications. Over time, additional data will greatly improve the accuracy and purity of current classifications. However, there appears to be a real need for a standard set of well-identified variable sources that can be used as a standard for testing the accuracy of automated methods. For example, large surveys such as LSST are expected to find millions of variable sources (Ivezic et al. 2008), whose classification will undoubtedly require the use of automated methods. In order to obtain reliable automated classifications as output, it is imperative to train these systems with accurately calibrated sets of priors.

8 DISCUSSION AND CONCLUSIONS

In this paper, we have presented an extensive search for periodic variable sources among 3.4 million candidate variables selected from the SSS data set. The resulting catalogue covers periodic variable sources over more of the Southern sky than any prior analysis. When combined with our recent analysis of CSS-N data (DR14), the resulting catalogues include ∼110 000 periodic variables across most of the visible sky (∼ 30 000deg^2).

During our analysis, we undertook an initial pre-classification process where we separated variable candidates into classes based on statistical parameters using MKDE and priors from DR14. This pre-selection allowed us to speed up the classification process. However, our visual inspection showed that this particular method did not reach the >90 per cent classification accuracy that we desired. In particular, the MKDE method requires a well-determined parameter space. This is not possible for variability classes that only include small numbers of members. Nevertheless, it is almost certainly possible to increase the classification accuracy by simply increasing thresholds to a level that guarantees almost all sources have a high S/N and are periodic. For example, DR14 found that setting the LS significance threshold to $\eta < 10^{-20}$ would lead to objects that had 95 per cent likelihood of being periodic. However, the use of such a criterion would mean that a very large fraction of the periodic variables were missed. This result requires careful consideration for future surveys that are aiming to maximize both completeness and accuracy while applying automated classification techniques.

Comparing the variable sources in this catalogue (along with SSS RRab's from Torrealba et al. 2015) with previously known periodic sources from VSX, we find a ∼95 per cent recovery rate for known periodic objects. However, ∼90 per cent of the ∼37 000 periodic variables in the catalogue are new discoveries. This is a much higher percentage than in DR14. The most likely reason for this, is that fewer synoptic surveys have been undertaken with coverage of these regions of the Southern sky.

As with DR14, we find many contact binaries that exhibit the O'Connell effect. The presence of stable light curves over >2000 d suggests that this effect is not due to star-spots. However, the presence of long-time-scale variations due to spots can be seen among some of the contact binary light curves.

8.1 Prospects for halo structure studies

We first announced the presence of extended halo of LMC RR Lyrae in Drake et al. (2016). That analysis revealed the presence of dozens of faint RRab's well beyond the limits of the LMC optical disc. Meanwhile, Belokurov & Koposov (2016) independently searched for halo structure near the LMC by selecting BHB candidates from DES data. In our current work, we have increased the number of LMC RRab's by using DES data to improve our RR Lyrae detection efficiency. Our results are in very good agreement with those of Belokurov & Koposov (2016), and suggest that the warm halo of

the LMC extends for more than 20°. However, the number of SSS RR Lyrae in our sample is insufficient to fully test whether the LMC stellar halo extends beyond 30° as suggested by Belokurov & Koposov (2016).

More recently, Belokurov et al. (2017) have used Gaia Data Release (GDR1) data to select likely variable sources with magnitudes and amplitudes consistent with Magellanic Cloud RR Lyrae. This data consist of tens of thousands of RR Lyrae candidates and also confirms that the LMC halo extends to at least ∼20°. However, there is currently insufficient public *Gaia* data to separate the RRab's from other types of variable sources with the same magnitudes and amplitudes. That is to say, QSOs and eclipsing binaries which were noted by Belokurov et al. (2017) to contribute 30–40 per cent contamination, or RR Lyrae of different pulsation types (e.g. RRc's and RRd's) that are not currently ideal distance tracers. In future, we plan to use SSS data to confirm many of the brighter RR Lyrae candidates of Belokurov et al. (2017).

Our combined Northern and Southern surveys have identified ∼43 500 RR Lyrae of all types (Drake et al. 2013a,b; DR14). The bulk of these (∼33 000) are RRab's and are currently being used to detect structure within the Galactic halo. In this analysis, we have also found many faint LPVs that are clearly associated with the LMC and nearby dwarf galaxies. Photometric follow-up of the regions surrounding the halo RRab's and LPVs could reveal the presence of faint dwarf galaxies since they were found to trace the Sagittarius dSph's tidal stream in DR14. Since our analysis these sources have been used to examine the extent of Magellanic Clouds using LPV candidates selected from GDR1 data (Deason et al. 2016). These objects show the presence of Mira candidates up to >12° from the LMC.

Many other halo tracers will be available for halo studies in the coming years, since to the combination of the *Gaia*, DES, and LSST surveys that will cover the entire Southern sky to unprecedented photometric precision and depth.

ACKNOWLEDGEMENTS

CRTS and CSDR1 are supported by the U.S. National Science Foundation under grants AST-1313422 and AST-1413600. The CSS survey is funded by the National Aeronautics and Space Administration under grant no. NNG05GF22G issued through the Science Mission Directorate Near-Earth Objects Observations Programme. AJD, MC, GT, VB, and SEK acknowledge partial support by CONICYT's PCI program through grant DPI20140066. MC is additionally supported by the Ministry for the Economy, Development, and Tourism's Iniciativa Científica Milenio through grant IC 120009, awarded to the Millennium Institute of Astrophysics; by Proyecto Fondecyt Regular no. 1141141; and by Proyecto Basal PFB-06/2007. This research has made use of the International VSX data base, operated at AAVSO, Cambridge, Massachusetts, USA, and the SIMBAD data base, operated at CDS, Strasbourg, France. AllWISE makes use of data from *WISE*, which is a joint project of the University of California, Los Angeles, and the Jet Propulsion Laboratory/California Institute of Technology, and NEOWISE, which is a project of the Jet Propulsion Laboratory/California Institute of Technology. *WISE* and NEOWISE are funded by the National Aeronautics and Space Administration.

The DES Data Management system is supported by the National Science Foundation under Grant Number (1138766) (Jarvis et al. 2016).

REFERENCES

Alcock C. et al., 1993, Nature, 365, 621
Alcock C. et al., 1996, ApJ, 482, 89
Alcock C. et al., 2000, ApJ, 536, 798
Atlee D. W., Gould A., 2007, ApJ, 664, 53
Balbinot E. et al., 2015, MNRAS, 449, 1129
Bellm E. C. et al., 2016, ApJ, 816, 74
Belokurov V., Koposov S. E., 2016, MNRAS, 456, 602
Belokurov V. et al., 2017, MNRAS, 466, 4711
Bertin E., Arnouts S., 1996, A&AS, 117, 393
Bessell M. S., 1969, ApJS, 18, 195
Blazhko S., 1907, Astron. Nachr., 175, 325
Borissova J., Minniti D., Rejkuba M., Alves D., 2006, A&A, 460, 459
Bowell E., Koehn B. W., Howell S. B., Hoffman M., Muinonen K., 1995, BAAS, 27, 1057
Breger M. et al., 2005, A&A, 435, 955
Butters O. W. et al., 2010, A&A 520, L10
Catelan M., 2009, Ap&SS, 320, 261
Catelan M., Smith H. A., 2015, Pulsating Stars, Wiley-VCH
Christlieb N., Beers T. C., Thom C., Wilhelm R, Rossi S., Flynn C., Wisotzki L., Reimers D., 2005, A&A, 431, 143
Clementini G. et al., 2016, A&A, 595, 133
Cortes C., Vapnik V., 1995, Mach. Learn., 20, 273
Deason A. J., Belokurov V., Erkal D., Koposov S. E., Mackey D., 2016, MNRAS, 467, 2636
Drake A. J., 2006, AJ, 131, 1056
Drake A. J. et al., 2013a, ApJ, 763, 32
Drake A. J. et al., 2013b, ApJ, 765, 154
Drake A. J. et al., 2014a, ApJS, 213, 9 (DR14)
Drake A. J. et al., 2014b, ApJ, 790, 157
Drake A. J. et al., 2014c, MNRAS, 441, 1186
Drake A. J. et al., 2016, AAS Meeting Abstracts, 227, 437.02
Dubath P. et al., 2011, MNRAS, 414, 2602
Elorrieta F. et al., 2016, A&A, 595, A82
Feldmeier J. J. et al., 2011, AJ, 142, 2
Freund Y., Schapire R. E., 1997, J. Comput. Syst. Sci., 55, 119
Gavrilchenko T., Klein C. R., Bloom J. S., Richards J. W., 2014, MNRAS, 441, 715
Gessner H., Meinunger I., 1974, Veroeff. Sternw. Sonneberg, 6, 249
Graham M. J., Drake A. J., Djorgovski S. G., Mahabal A. A., Donalek C., Duan V., Maker A., 2013, MNRAS, 434, 3423
Graham M. J. et al., 2015, Nature, 518, 74
Hartman J. D., Bakos G. A., Noyes R. W., Sipocz B., Kovacs G., Mazeh T., Shporer A., Pal A., 2011, AJ, 141, 166
Himpel K., 1944, BZ, 26, 25
Hoffmeister C., 1963, Veroeff. Sternw. Sonneberg, 6, 1
Huxor A. P., Grebel E. K., 2015, MNRAS, 453, 2653
Ivezic Z. et al., 2008, preprint (arXiv:0805.2366)
Jarvis M. et al., 2016, MNRAS, 460, 2245
Jurcsik J., Smitola P., Hajdu G., Nuspl J., 2014, ApJL, 797, 3
Jurcsik J. et al., 2015, ApJS, 219, 25
Kim D.-W., Protopapas P., Bailer-Jones C. A. L., Byun Y.-I., Chang S.-W., Marquette J.-B., Shin M.-S., 2014, A&A, 566, 43
Kinemuchi K., Smith H. A., Wozniak P. R., McKay T. A., 2006, AJ, 132, 1202
Kollmeier J. A. et al., 2013, ApJ, 775, 57
Larson S., Beshore E., Hill R., Christensen E., McLean D., Kolar S., McNaught R., Garradd G., 2003, BAAS, 35, 36.04
Lee C.-H., 2015, MNRAS, 454, 2946
Lee Y.-H., Kim S. S., Shin J., Lee J., Jin H., 2008, PASJ, 60, 551
Lomb N. R., 1976, Ap&SS, 39, 447
Mackey D., Koposov S. E., Erkal D., Belokurov V., Da Costa G. S., Gomez F. A., 2016, MNRAS, 459, 239
Maintz G., 2005, A&A, 442, 381
Mainzer A. et al., 2011 ApJ, 731, 53
Majewski S. R., Nidever D. L., Munoz R. R., Patterson R. J., Kunkel W. E., Carlin J. L., 2009, in Van Loon J. T. Oliveira M., eds, Proc. IAU Symp.

256, The Magellanic System: Stars, Gas, and Galaxies. Cambridge Univ. Press, Cambridge, p. 51
Marsh F. M., Prince T. A., Mahabal A. A., Bellm E. C., Drake A. J., Djorgovski S. G., 2016, MNRAS, 465, 4678
Martin D. C. et al., 2005, ApJL, 619, 1
Masci F. J., Hoffmann D. I., Grillmair C. J., Cutri R. M., 2014, AJ, 148, 21
McNamara D. H., 1995, AJ, 109, 2134
Mennessier M. O., Colome J., 2002, A&A, 390, 173
Miceli A. et al., 2008, ApJ, 678, 865
Minniti D., Borissova J., Rejkuba M., Alves D. R., Cook K. H., Freeman K. C., 2003, Science, 301, 1508
Minniti D. et al., 2010, New Astron., 15, 433
Momany Y., Held E. V., Saviane I., Zaggia S., Rizzi L., Gullieuszik M., 2007, A&A 468, 973
O'Connell D. J. K., 1951, Pub. Riverview Coll. Obs., 2, 85
Paggi A., Massaro F., D'Abrusco R., Smith H. A., Masetti N., Giroletti M., Tosti G., Funk S., 2013, ApJS, 209, 9
Palaversa L. et al., 2013, AJ, 146, 101
Pietrzynski G. et al., 2013, Nature, 495, 76
Pojmanski G., 1997, Acta Astron., 47, 467
Pojmanski G., 2000, Acta Astron., 50, 177
Pojmanski G., 2002, Acta Astron., 52, 397
Pojmanski G., 2003, Acta Astron., 53, 341
Pojmanski G., Maciejewski G., 2004a, Acta Astron., 54, 153
Pojmanski G., Maciejewski G., 2004b, Acta Astron., 55, 97
Pojmanski G., Pilecki B., Szczygiel D., 2005, Acta Astron., 55, 275
Pritzl B. J., Smith H. A., Stetson P. B., Catelan M., Sweigart A. V., Layden A. C., Rich R. M., 2003, AJ, 126, 1381
Richards J. W. et al., 2011, ApJ, 733, 10
Richards J. W., Starr D. L., Miller A. A., Bloom J. S., Butler N. R., Brink H., Crellin-Quick A., 2012, ApJS, 203, 32
Roberts M. S. E., 2013, in van Leeuwen J., ed., Proc. IAU Symp. 291, Neutron Stars and Pulsars.Cambridge Univ. Press, Cambridge, p. 127
Romani R. W., Shaw M. S., 2011, ApJL, 743, 26
Rucinski S. M., 1992, AJ, 103, 960
Rucinski S. M., 1997, MNRAS, 382, 393
Saha A. et al., 2010, AJ, 140, 1719
Samus N. N. et al., 2003, Astron. Lett., 29, 468
Sandage A., Tammann G. A., 2006, ARA&A, 44, 93
Scargle J. D., 1982, ApJ, 263, 835
Schwarzenberg-Czerny A., 1996, ApJL, 460, 107
Scott D. W., 2015, Multivariate Density Estimation: Theory, Practice, and Visualization, Wiley, Hoboken, NJ
Sesar B. et al., 2013, AJ, 146, 21
Sesar B. et al., 2017, AJ, 153, 204
Shishayeva M. N., Kholopov P. N., 1977, Perem. Zvezdy Prilozhenie, 3, 271
Soszyński I. et al., 2008, Acta Astron., 58, 293
Soszyński I. et al., 2009, Acta Astron., 59, 1
Soszyński I. et al., 2013, Acta Astron., 63, 21
Soszyński I. et al., 2015, Acta Astron., 65, 233
Soszyński I. et al., 2016, Acta Astron., 66, 131
Stetson P. B., 1996, PASP, 108, 851
Stokes G. H., Evans J. B., Viggh H. E. M., Shelly F. C., Pearce E. C., 2000, Icarus, 148, 21
Tam P. H. T. et al., 2010, ApJL, 24, 207
Torrealba G. et al., 2015, MNRAS, 446, 2251
Udalski A. Szymanski M., Kaluzny J., Kubiak M., Mateo M., Krzeminski W., 1994, ApJ, 426, 69
van der Marel R. P., 2001, AJ, 122, 1827
van der Marel R. P., Alves D. R., Hardy E., Suntzeff N. B., 2002, AJ, 124, 2639
van der Marel R. P., Kallivayalil N., 2014, ApJ, 781, 121
Vennes S., Kawka A., Nemeth P., 2011, MNRAS, 410, 2095
Wallerstein G., 2002, PASP, 114, 689
Wang Z. Archibald A. M., Thorstensen J. R., Kaspi V. M., Lorimer D. R., Stairs I., Ransom S. M., 2009, ApJ, 703, 2017
Watson C., 2006, J. Am. Assoc. Var. Star Obs., 35, 318
Wenger M. et al., 2000, A&AS, 143, 9
Wils P., Kleidis S., Broens E., 2008, MNRAS, 387, 783
Wilsey N. J., Beaky M. M., 2009, Soc. Astron. Sci. Annu. Symp., 28, 107
Zhang X.-B., Deng L.-C., Xin Y., Zhou X., 2003, Chin. J. Astron. Astrophys. (ChJAA), 3, 151

SUPPORTING INFORMATION

Supplementary data are available at *MNRAS* online.

Table 4. Periodic variable catalogue.

Please note: Oxford University Press is not responsible for the content or functionality of any supporting materials supplied by the authors. Any queries (other than missing material) should be directed to the corresponding author for the article.

APPENDIX A: INCREASING LMC RRAB DETECTION COMPLETENESS WITH DES

The selection of RRab's at the distance of the LMC from SSS data is limited by the S/N required to select objects that are both variable and periodic. However, RRab's at the distance of the LMC have a limited range of median magnitudes and colours. It is thus possible to select candidate LMC RRab's in the outer halo by using magnitude and colour combined with variability. Therefore, we used the deep photometry provided by Dark Energy Survey Science Verification-1 data set (DES-SVA1)[4] to select RRab candidates based on their magnitude and colour. We then cross-matched these sources to the list of all variable star candidates in SSS data.

The first step was to select all DES-SVA1 sources near the LMC ($50^\circ < \alpha < 150^\circ$ and $\delta < -30^\circ$). By cross-matching these sources with the known LMC RRab's from our catalogue, we found 28 RRab's with DES photometry. We determined that the range of expected RRab magnitudes and colours based on these sources is $18.3 < r < 19.7$, $-0.2 < g - r < 0.4$, $-0.6 < r - i < 0.5$, and $-0.35 < i - z < 0.25$. The colour range is much broader than we found in our previous match with SDSS in DR14 since, unlike SDSS, each of the DES observations will generally be taken at very different pulsation phases. These colour cuts select 39 081 DES sources from among the 400 thousand DES-SVA1 sources in the magnitude range.

Matching these with SSS variable candidates, we got 1587 matches to the 3.46 million SSS variable candidates. Since LMC RRab's have a relatively low S/N in SSS data, large numbers of observations are required to find reliable periods. We removed all SSS variable candidates having less than 80 detections. We also removed matches where the median magnitude of the matched SSS stars was brighter than V=18 (as most of these are blends). The total number of variable candidates was reduced to 1075.

We ran the AFD process (Torrealba et al. 2015) on all of these sources and 226 had best-fitting periods in the RRab range ($0.43 < P[d] < 0.95$). This selection included the 28 RRab's that we had previously discovered. By inspecting the light curves of the 226 candidates, we identified 31 additional LMC RRab's within the DESVA1 footprint. In Table A1, we give parameters of these RRab's. In Fig. A1, we present examples of the phased light curves of these RRab's. Compared to Fig. 17, these sources are slightly noisier. Nevertheless, they are clearly RRab's.

[4] https://des.ncsa.illinois.edu/releases/sva1

Table A1. Parameters of LMC RRab's selected using SSS and DES data. Column (1) Catalina ID. Columns (2) and (3) right ascension and declination. Column (4) Period from AFD. Column (5) Median CSS V magnitude. Column (6) Number of points in SSS light curve. Columns (7)–(10) DES g, r, i, and z magnitudes, respectively.

CRTS ID	RA	Dec. (J2000)	P (d)	$V_{\rm med}$	N	g	r	i	z
SSS_J042430.1−450232	04:24:30.12	−45:02:32.3	0.647439	18.78	175	18.77	18.79	18.84	18.91
SSS_J043052.6−593801	04:30:52.64	−59:38:01.4	0.604634	18.82	142	19.36	19.05	19.02	18.93
SSS_J043151.2−604821	04:31:51.24	−60:48:21.2	0.555255	18.96	100	19.34	19.12	19.10	19.10
SSS_J043233.3−581446	04:32:33.34	−58:14:46.5	0.563902	18.72	150	18.93	18.79	18.92	18.90
SSS_J043303.1−565344	04:33:03.19	−56:53:44.0	0.49585	19.18	92	19.88	19.66	19.63	19.62
SSS_J043404.8−571051	04:34:04.86	−57:10:51.8	0.63388	19.00	123	19.54	19.29	19.00	18.98
SSS_J044141.8−605402	04:41:41.80	−60:54:02.0	0.477490	18.77	98	19.27	19.09	19.28	19.27
SSS_J044235.0−551400	04:42:35.03	−55:14:00.2	0.544473	19.19	122	19.73	19.46	19.35	19.34
SSS_J044321.9−600333	04:43:21.98	−60:03:33.5	0.547652	19.00	92	18.90	18.91	19.30	19.29
SSS_J044611.9−601559	04:46:11.94	−60:15:59.8	0.62372	19.02	121	19.51	19.24	19.06	19.06
SSS_J044617.7−590008	04:46:17.75	−59:00:08.2	0.63730	18.84	128	18.89	18.77	18.76	18.68
SSS_J044823.4−572536	04:48:23.47	−57:25:36.5	0.60834	18.84	138	19.36	19.11	18.97	18.90
SSS_J045749.4−575050	04:57:49.43	−57:50:50.8	0.490367	18.94	129	19.48	19.17	19.26	19.25
SSS_J045753.5−601458	04:57:53.58	−60:14:58.7	0.64279	18.52	116	18.55	18.46	18.44	18.35
SSS_J050103.8−580358	05:01:03.80	−58:03:58.0	0.69206	18.78	157	18.73	18.64	19.10	19.09
SSS_J050107.8−601559	05:01:07.87	−60:15:59.3	0.608515	18.65	140	18.77	18.68	18.73	18.64
SSS_J050245.5−571023	05:02:45.53	−57:10:23.2	0.588125	18.89	131	19.18	19.05	18.95	18.98
SSS_J050817.6−564837	05:08:17.60	−56:48:37.1	0.46117	18.76	94	19.39	19.25	19.06	19.02
SSS_J051029.4−551044	05:10:29.47	−55:10:44.6	0.602485	18.81	116	18.86	18.78	18.62	18.62
SSS_J052317.7−571521	05:23:17.76	−57:15:21.7	0.525028	18.74	150	19.60	19.33	19.19	19.17
SSS_J052331.0−572534	05:23:31.08	−57:25:34.9	0.575638	19.02	140	19.36	19.11	18.92	18.87
SSS_J052653.8−600033	05:26:53.80	−60:00:33.3	0.517786	18.72	126	19.28	19.01	18.96	18.80
SSS_J052758.9−553444	05:27:58.94	−55:34:44.4	0.62058	19.31	111	18.88	18.91	19.47	19.46
SSS_J052924.4−600406	05:29:24.43	−60:04:06.6	0.508405	18.98	118	19.54	19.16	18.87	18.83
SSS_J053156.6−590932	05:31:56.62	−59:09:32.2	0.509650	18.98	105	19.01	19.06	18.90	18.86
SSS_J053320.4−602637	05:33:20.46	−60:26:37.0	0.58018	19.04	126	19.18	18.92	18.88	19.02
SSS_J053415.0−572120	05:34:15.02	−57:21:20.6	0.491355	18.85	109	19.51	19.32	19.28	19.27
SSS_J054322.6−600035	05:43:22.67	−60:00:35.4	0.566284	18.93	131	18.86	18.78	19.06	19.01
SSS_J054338.0−580741	05:43:38.04	−58:07:41.7	0.512098	18.74	161	19.05	19.16	19.07	19.07
SSS_J054603.7−573331	05:46:03.76	−57:33:31.5	0.564825	18.96	149	18.91	18.70	18.84	18.83
SSS_J054744.0−601138	05:47:44.05	−60:11:38.6	0.562772	18.94	150	19.00	18.95	18.89	18.87

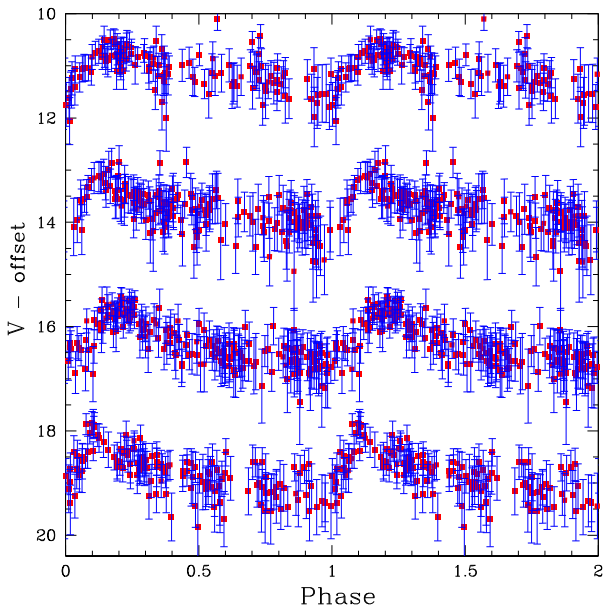

Figure A1. The light curves of LMC RRab selected using colour and magnitude cuts based on DES DR1 photometry. From bottom to top these are: SSSJ052653.8−600033 (0.518 d), SSSJ054338.0−580741 (0.512 d), SSSJ054603.7−573331 (0.565 d), and SSSJ045753.5−601458 (0.643 d). The top three light curves have been offset by 2.5, 5.2, and 7.5 mag to avoid confusion due to overlap.

The discovery of these additional outer LMC RRab's confirms that the LMC halo extends to at least 20° from the LMC centre. However, only one of the 31 new RRab's is beyond 20° even though approximately half of the initial DES-selected candidates were. This suggests that additional LMC RRab's could be found in the outer regions of the LMC by adding addition area covered be more recent DES data. Nevertheless, this sample is unlikely to be very complete due to the limited depth of the SSS data.

APPENDIX B: CATACLYSMIC VARIABLES

During inspection of the periodic candidates in this work, we discovered 136 non-periodic sources where the light curve showed outbursts or high-amplitude rapid variability. 61 of these sources had matches to VSX and 13 to SIMBAD. Most of these objects were known dwarf novae types. The remaining 75 sources have similar light curves to the previously identified dwarf novae as well as those given in Drake et al. (2014c).

In Table B1, we present the details for 75 new CV candidates discovered during this analysis. The identification is less certain than for many of the CVs given in DR14 due to the lack of SDSS photometry. However, many of them are associated with moderately bright UV sources detected by *GALEX*. Given that these sources are generally not periodic, yet were found among objects selected as possible periodic variables, we are certain that a very large number of CVs remain to be detected among the SSS variables.

Table B1. Parameters of newly discovered CVs.

CRTS ID	RA	Dec. (J2000)	$V_{\rm med}$	NUV	FUV
SSS_J011113.4−444134	01:11:13.48	−44:41:34.4	17.83	18.154	18.297
SSS_J012426.0−513855	01:24:26.06	−51:38:55.7	17.65	19.080	19.297
SSS_J022157.0−605540	02:21:57.01	−60:55:40.8	16.72	–	–
SSS_J024350.4−291239	02:43:50.44	−29:12:39.5	16.99	–	–[a]
SSS_J035055.8−204817	03:50:55.88	−20:48:17.2	14.50	17.626	18.068
SSS_J044348.7−594906	04:43:48.78	−59:49:06.1	18.15	–	–
SSS_J052113.9−520258	05:21:13.92	−52:02:58.4	15.35	–	–
SSS_J052121.5−280532	05:21:21.56	−28:05:32.5	15.53	17.756	17.717
SSS_J053256.0−283730	05:32:56.01	−28:37:30.2	17.84	19.032	19.442
SSS_J060211.7−394732	06:02:11.78	−39:47:32.4	14.64	–	–
SSS_J061558.6−515424	06:15:58.68	−51:54:24.1	14.86	–	–[a]
SSS_J062053.6−324645	06:20:53.65	−32:46:45.3	16.15	–	–
SSS_J062321.5−354053	06:23:21.56	−35:40:53.9	15.70	18.328	18.167
SSS_J063215.3−544258	06:32:15.37	−54:42:58.6	17.96	–	–[a]
SSS_J063248.9−523227	06:32:48.98	−52:32:27.5	16.33	–	–[a]
SSS_J064307.9−403011	06:43:07.96	−40:30:11.1	16.39	–	–
SSS_J064532.8−283232	06:45:32.83	−28:32:32.2	16.16	–	–[a]
SSS_J065150.8−351938	06:51:50.86	−35:19:38.7	17.71	–	–
SSS_J065723.6−392811	06:57:23.64	−39:28:11.4	17.66	–	–
SSS_J065847.5−485239	06:58:47.53	−48:52:39.1	18.32	–	–
SSS_J070312.4−693819	07:03:12.45	−69:38:19.8	18.00	–	–
SSS_J080833.0−515136	08:08:33.07	−51:51:36.1	16.14	–	–[a]
SSS_J081800.1−511936	08:18:00.11	−51:19:36.8	17.53	–	–[a]
SSS_J085507.4−211809	08:55:07.40	−21:18:09.6	17.79	20.375	21.160
SSS_J091040.2−324126	09:10:40.20	−32:41:26.7	16.02	–	–[a]
SSS_J092612.7−310843	09:26:12.75	−31:08:43.6	14.28	15.337	15.449
SSS_J093714.4−400442	09:37:14.45	−40:04:42.1	17.49	–	–
SSS_J094321.5−395918	09:43:21.51	−39:59:18.3	14.77	–	–
SSS_J095049.4−412322	09:50:49.49	−41:23:22.6	16.12	16.771	17.041
SSS_J095725.1−355239	09:57:25.15	−35:52:39.3	16.39	–	–
SSS_J095832.7−274950	09:58:32.72	−27:49:50.7	18.99	21.316	21.218
SSS_J095943.1−401207	09:59:43.19	−40:12:07.8	18.54	–	–
SSS_J100328.4−382022	10:03:28.45	−38:20:22.5	16.40	18.656	18.679
SSS_J102416.9−425352	10:24:16.91	−42:53:52.8	17.60	21.666	21.154[a]
SSS_J110529.7−400705	11:05:29.71	−40:07:05.7	15.34	16.161	16.286
SSS_J110808.8−495228	11:08:08.82	−49:52:28.7	17.06	–	–
SSS_J110909.0−415331	11:09:09.00	−41:53:31.8	14.04	–	–
SSS_J110917.9−202434	11:09:17.93	−20:24:34.8	18.45	19.352	19.511
SSS_J113315.3−371020	11:33:15.36	−37:10:20.7	16.52	17.198	17.403
SSS_J120849.3−304136	12:08:49.30	−30:41:36.7	16.53	16.516	16.802[a]
SSS_J123622.2−404812	12:36:22.21	−40:48:12.4	18.01	–	–
SSS_J124523.4−350956	12:45:23.40	−35:09:56.7	16.54	16.682	16.480
SSS_J130804.8−414624	13:08:04.86	−41:46:24.7	17.12	19.604	19.900
SSS_J132149.2−330958	13:21:49.20	−33:09:58.6	18.04	19.488	21.317
SSS_J134421.2−344948	13:44:21.21	−34:49:48.0	16.03	–	–
SSS_J140952.9−364133	14:09:52.93	−36:41:33.5	16.25	–	–
SSS_J143037.9−405759	14:30:37.91	−40:57:59.9	18.09	–	–
SSS_J152419.6−350030	15:24:19.61	−35:00:30.4	16.39	–	–
SSS_J154801.4−292511	15:48:01.42	−29:25:11.1	17.92	–	–
SSS_J155147.2−211323	15:51:47.21	−21:13:23.0	16.72	–	–[a]
SSS_J155929.1−223618	15:59:29.15	−22:36:18.2	16.54	–	–
SSS_J160058.3−243818	16:00:58.39	−24:38:18.7	18.19	–	–
SSS_J160805.5−285642	16:08:05.53	−28:56:42.7	16.86	–	–
SSS_J161848.7−220642	16:18:48.79	−22:06:42.3	15.98	–	–[a]
SSS_J162131.9−230140	16:21:31.97	−23:01:40.3	16.08	–	–[a]
SSS_J162318.1−262543	16:23:18.10	−26:25:43.2	16.06	–	–[a]
SSS_J162837.1−282656	16:28:37.12	−28:26:56.1	17.13	–	–[a]
SSS_J163111.2−282648	16:31:11.24	−28:26:48.9	16.72	–	–
SSS_J163641.4−222346	16:36:41.48	−22:23:46.8	18.56	–	–
SSS_J165258.1−231044	16:52:58.15	−23:10:44.0	17.12	18.993	19.146
SSS_J182313.7−604107	18:23:13.73	−60:41:07.0	18.09	–	–
SSS_J183606.2−504742	18:36:06.26	−50:47:42.9	17.94	21.088	21.222
SSS_J192554.8−461901	19:25:54.82	−46:19:01.6	16.88	16.809	16.799
SSS_J192909.1−354245	19:29:09.13	−35:42:45.5	18.15	19.311	19.760

Table B1 – *continued*

CRTS ID	RA	Dec. (J2000)	$V_{\rm med}$	NUV	FUV
SSS_J193504.8−574934	19:35:04.83	−57:49:34.7	18.15	–	–
SSS_J194038.2−330745	19:40:38.27	−33:07:45.6	17.44	–	–[a]
SSS_J194622.6−403359	19:46:22.61	−40:33:59.6	18.21	19.376	19.537[a]
SSS_J195635.3−532601	19:56:35.39	−53:26:01.6	18.71	19.815	19.997
SSS_J200409.4−280008	20:04:09.48	−28:00:08.2	17.53	18.510	18.345
SSS_J203248.8−295521	20:32:48.85	−29:55:21.2	17.95	–	–
SSS_J205621.5−315239	20:56:21.57	−31:52:39.6	18.04	–	–[a]
SSS_J214830.4−353848	21:48:30.43	−35:38:48.9	18.14	–	–
SSS_J220218.9−430519	22:02:18.90	−43:05:19.0	14.74	14.906	16.438
SSS_J220630.7−524420	22:06:30.79	−52:44:20.7	16.53	16.340	18.330
SSS_J225920.6−253529	22:59:20.68	−25:35:29.4	18.79	–	–

Column (1) Catalina ID. Columns (2) and (3) right ascension and declination Column (4) median CSS magnitude. Columns (5) and (6) *GALEX* NUV and FUV magnitudes, respectively.
[a]The identification is uncertain.

This paper has been typeset from a TEX/LATEX file prepared by the author.